Draft version November 5, 2017
Typeset using LaTeX default style in AASTeX61

KINEMATICS OF THE HORSEHEAD NEBULA & IC 434 IONIZATION FRONT IN CO AND [C$^+$]

John Bally,[1] Ed Chambers,[2] Viviana Guzman,[3] Eric Keto,[4] Bhaswati Mookerjea,[5] Goran Sandell,[6] Thomas Stanke,[7] and Hans Zinnecker[8,9]

[1] *Center for Astrophysics and Space Astronomy, Astrophysical and Planetary Sciences Department, University of Colorado, UCB 389 Boulder, Colorado 80309, USA*
[2] *USRA/SOFIA, NASA Ames Research Center, Mail Stop 232-12, Building N232, P.O. Box 1, Moffett Field, CA 94035-0001*
[3] *Joint ALMA Observatory, Avenida Alonso de Cordova 3107, Vitacura, Santiago, Chile*
[4] *Center for Astrophysics, Cambridge, MA*
[5] *AA(Tata Institute of Fundamental Research, Homi Bhabha Road, 400005, Mumbai, India*
[6] *Institute for Astronomy, 640 N. Aohoku Pl, Hilo, HI 96720*
[7] *European Southern Observatory, Garching-bei Munchen, Germany*
[8] *Deutsches SOFIA Institut (DSI), University of Stuttgart, Pfaffenwaldring 29, 70569, Germany*
[9] *Universidad Autonoma de Chile, Chile*

(Received July 1, 2017; Revised September 27, 2017)

Submitted to ApJ

ABSTRACT

New SOFIA [C$^+$] 157 μm, APEX 860 μm J=3−2 CO, and archival JCMT J=2−1 CO and ^{13}CO observations of the Horsehead Nebula are presented. The photon-dominated region (PDR) between the Orion B molecular cloud and the adjacent IC 434 HII region are used to study the radial velocity structure of the region and the feedback impacts of UV radiation. Multiple west-facing cloud edges are superimposed along the line of sight with radial velocities which differ by a few km s^{-1}. The Horsehead lies in the foreground blueshifted portion of the Orion B molecular cloud and is predominantly illuminated from the rear. The mean H_2 density of the Horsehead, $\sim 6 \times 10^3$ cm^{-3}, results in a spatially thin PDR where the photo-ablation flow has compressed the western cloud edge to an H_2 density of $2-6\times10^4$ cm^{-3}. The associated [C$^+$] 157 μm layer has a width L<0.05 pc. The background parts of the Orion B cloud in the imaged field consist of a clumpy medium surrounded by molecular gas with H_2 densities lower by one to two orders of magnitude. Along the straight part of the IC 434 ionization front, the PDR layer probed by [C$^+$] 157 μm emission is much thicker with L∼0.5 pc. A possible model for the formation and evolution of this edge-on ionization front and PDR is presented. **The [C$^+$] data was independently analyzed and published by Pabst et al. (2017)**

Keywords: ISM: photon dominated regions; ISM: individual objects: Horsehead Nebula ISM: individual objects: Barnard 33

Corresponding author: John Bally
john.bally@colorado.edu

1. INTRODUCTION

Ultraviolet (UV) radiation from massive stars injects energy and momentum into the surrounding ISM, contributes to cloud dispersal and destruction, but can also trigger star formation (Tielens & Hollenbach 1985; Hollenbach & Tielens 1999; Elmegreen & Lada 1977). For gas-to-dust ratios similar to the Solar vicinity, UV with wavelengths longer than 912 Å but less than about 2,000 Å (far-UV or FUV) which does not ionize hydrogen, can heat cloud surface layers to a depth where the hydrogen column density is less than $N(HI + H_2) \lesssim 10^{21}$ cm^{-2} to temperatures of hundreds to thousands of Kelvins, depending on the incident FUV flux. The penetration depth of this radiation is mostly set by the attenuation of the radiation field by the dust. Heating is dominated by photo-electrons ejected by irradiated grains with energies of a few eV, and the dissociation of H_2 followed by re-formation on grain surfaces and ejection with a kinetic energy of a few eV. Heated gas will expand away from the cloud surface towards the UV source at roughly the local sound-speed, $c_s = (kT/\mu m_H)^{1/2}$ ~1 to 5 km s^{-1}. Momentum conservation implies that a weak shock or subsonic pressure pulse will compress and accelerate the colder cloud surface layers interior to the heated layer in a direction away from the UV source (Bertoldi & Draine 1996).

Extreme-UV (EUV) radiation with λ <912Å ionizes hydrogen and heats the expanding FUV-heated neutral flow to a temperature of order 10^4 K, accelerating it to ~5 − 20 of km s^{-1}. Ionization-induced heating results in a pressure jump which drives a D-type shock front into the cloud. The shock can impart motions of a few km s^{-1} away from the UV source, compressing the post-shock cold gas. The pressure of the incident radiation itself can impart additional acceleration away from the UV source under certain conditions. Thus, EUV, FUV, and radiation pressure can accelerate cold cloud surface layers in a direction opposite to the expanding, heated layers. Although diverging heating and ionization fronts (I-fronts) can dissociate, accelerate, and disperse clouds, converging I-fronts can be compressive, triggering gravitational collapse and star formation. Thus, UV feedback can generate chaotic motions and turbulence, disrupt clouds, or trigger star formation (Garcia-Segura & Franco 1996; Hosokawa & Inutsuka 2006a; 2006b).

The iconic Horsehead Nebula in Orion (Barnard 33) is a dense, dark cloud protruding from the western rim of the southwest portion of the Orion B (Lynds 1630) molecular cloud into the IC 434 HII region ionized by σ-Ori located ~4 pc to the west in projection. **σ-Ori is a multiple system containing stars with spectral types O9.5, B0.5, two B2, and an A2 star with a combined Lyman continuum luminosity of Q≈ 1.6×10^{48} EUV photons s^{-1} and a total luminosity L≈ 7.6×10^4 L$_\odot$, the bulk of which emerges in the FUV band. The illumination of the IC 434 ionization front also contains a contribution from a half-dozen other B- and A stars type stars, whose spectral energy distributions peak in the FUV. Thus, the FUV luminosity of the σ-Ori cluster is L(FUV) ≈ 2×10^{49} FUV photons s^{-1} which produces an FUV flux of about F_{FUV} ≈ 0.15 erg s^{-1} cm^{-2} = 100 G$_0$ (Abergel, 2003; G$_0$ = 1.5×10^{-3} erg s^{-1}cm^{-2} is the Habing field) at a distance of 4 pc from σ-Ori.**

The Horsehead and IC 434 I-front is an ideal environment in which to quantify feedback processes in a relatively weak radiation environment far more typical than the intense radiation environment of the well studied Orion Nebula (Andree-Labsch et al. 2017; Pérez-Beaupuits et al. 2012; Pellegrini et al. 2009; Goicoechea et al. 2016). The Horsehead is seen in silhouette against the diffuse, degree-scale IC 434 HII region (Figure 1) that provides a relatively well-constrained illumination geometry. The I-front and associated photon dominated region (PDR) are close to edge-on, simplifying the interpretation of its stratified structure. Figure 2 shows a cartoon of the likely configuration.

Because the Horsehead is seen in silhouette against IC 434, it must be somewhat in front of σ-Ori which is thought to be at a distance of 330 to 385 pc. Mookerjea et al. (2009) argued that the most likely distance to the Horsehead is around 350 pc. However, radio parallax measurements to stars in the NGC 2024 HII region, located about 6 pc north of the Horsehead (in projection), indicate a distance to this part of Orion B of about 423±15 pc (Kounkel et al. 2017). Gaia DR1 (Gaia Collaboration et al. 2016) gives a distance of 360±35 pc to HD37903, the illuminator of the NGC 2023 reflection nebula located about 2 pc (in projection) north-northeast of the Horsehead. Thus, we adopt a distance of 360 pc to the Horsehead.

The Orion B cloud has been surveyed with increasing resolution over the past decades (Bally et al. 1987; Lada et al. 1991; Pound et al. 2003; Pety et al. 2012, 2017). Molecular line studies of the Horsehead include Pound et al. (2003) who presented single-dish and interferometer studies in CO J=1−0 and found a mass of 27 M$_\odot$ and a mean H_2 density 5×10^3 cm^{-3}. Hily-Blant et al. (2005) mapped C^{18}O 2-1, finding that the core of the Horsehead contains a 0.15 pc wide, clumpy filament which rotates about its major axis with a period ~4 Myr. Star formation in the southwestern part of Orion B was studied by Megeath et al. (2012, 2016). The Horsehead Nebula contains several young stars

with the most prominent located in the PDR along the western rim (Reipurth & Bouchet 1984; Bowler et al. 2009; Mookerjea et al. 2009).

Goicoechea et al. (2009) found a strong gradient in the ionization fraction through the PDR along the western, anvil-shaped 'nose' and 'mane' that contains the PDR along the western rim of the Horsehead. Abergel et al. (2003) used ISOCAM on ISO to image the Horsehead in the 5 to 18 μm wavelength range, finding strong mid-IR emission along a thin, 0.05 pc wide PDR along its western rim. Strong mid-IR H_2 emission in this region was mapped with Spitzer/IRS (Habart et al. 2011).

The molecular content of the Horsehead PDR has been extensively studied with the IRAM 30-meter and PdBI interferometers. Guzmán et al. (2011), Guzmán et al. (2013), Gratier et al. (2013), and Guzmán et al. (2015) found complex organics such as H_2CO, CH_3OH, CH_3CN, CH_2CO, CH_3CHO, and others which suggests that production of these species occurs via grain surface reactions in the UV-dominated PDR. Guzmán et al. (2012a) and Guzmán et al. (2012b) detected CF^+ in the PDR and show that this molecular ion forms there by the reaction of C^+ with HF. Thus, the [C^+] 157 μm emitting layer in the PDR co-exists with molecules.

The vicinity of the Horsehead Nebula was first mapped in [C^+] line with 0.9 meter telescope on-board the Kuiper Airborne Observatory (Zhou et al. 1993) **using the 5 by 5 pixel FIFI Fabry-Perot spectrometer. They present a map of a 7′ by 7′ field covering the Horsehead protrusion with a spatial resolution of 68″ and a spectral resolution of 51 km s^{-1} showing the total intensity of the [C^+] emission.** In this paper, we present observations of the Horsehead Nebula and the adjacent ionization front and PDR in the [C^+] line obtained with GREAT on SOFIA and CO J=3-2 data obtained with APEX. We use the constrained illumination geometry (Figure 2) to relate the radial velocity structure traced by CO and C^+ to investigate the feedback impacts and accelerations produced by external ionization. **Pabst et al. (2017) published an analysis of the Horsehead Nebula based on the same [C^+] 157 μm data used for this analysis.**

2. OBSERVATIONS

2.1. *SOFIA*

The Horsehead region was observed as a science demonstration project on December 11, 2015 with GREAT onboard the Stratospheric Observatory for Infrared Astronomy (SOFIA). GREAT is a dual channel heterodyne receiver with both channels operating simultaneously. At the time GREAT was in the Low Frequency Array (LFA)/L1 configuration with the LFA tuned to [CII] (1.9005396 THz) and L1 tuned to CO(11-10). THE LFA is a 2 x 7 pixel array in two orthogonal polarizations in a hexagonal configuration with one central pixel, i.e., a total of 14 pixels. The spacing between the pixels is two beam widths or ∼33″. For more detailed information about the LFA, see Risacher et al. (2016).

The observations were done on a 4.2 hour leg at an altitude 43,000 feet. The 12.5′ × 17.5′ field, tilted by −10 deg, was observed with the array On-The-Fly (OTF) total power mode with the off position at −733″, +27.5″ relative to the Horsehead position (RA = 05:40:54.27, DEC = −02:28:00 (2000). In the array mapping mode the second channel (L1) is severely under sampled and did not produce any usable data. The observed area was divided into four slightly overlapping subfields, each of which were observed twice. Each submap was observed once in the array OTF mode, i.e., the array was rotated −19.1° relative to the scan direction with a sampling rate of 0.4 seconds per 6″ and then scanned again with a step of 5.5″ in the orthogonal direction to obtain a fully sampled map. Each submap was also scanned the same way in the orthogonal direction with a sampling rate of 0.3 seconds per 6″. Once the four submaps were completed the array was rotated by 60 deg and the whole process was repeated. This ensured that every point in the map is covered by all pixels.

The data were calibrated and reduced by the GREAT team and provided to the user community as CLASS data cubes. The beam size of the LFA is ∼15.1″ and the average beam efficiency, η_{mb} ∼0.68. The average receiver temperature (DSB) was about 1000 K per pixel, excluding two mixers which had higher receiver temperatures due to insufficient LO power. **The final data cube has a channel spacing of 0.193 km s^{-1}. These data were averaged and re-sampled into ∼0.5 and 1.0 km s^{-1} wide velocity channels to improve the signal-to-noise ratio.** The data has an rms noise temperature about 1.2 K (T_{mb}) for a channel width of 0.5 km s^{-1}.

2.2. *APEX*

The 345 GHz ^{12}CO J=3-2 data used here was obtained with the 12-m APEX telescope as part of the APEX Large CO Heterodyne Orion Legacy Survey (ALCOHOLS; P.I. T. Stanke). ALCOHOLS used the 64-pixel heterodyne

camera, SuperCam (Kloosterman et al. 2012), to survey the Orion A (south) and B clouds with an angular resolution of ∼15″ well-matched to the angular resolution of the SOFIA GREAT observations with a beam-diameter of ∼18″. The spectral resolution of the data used here is 0.25 km s^{-1} and the r.m.s. noise is ∼0.25 Kelvin per channel.

2.3. *JCMT*

The Horsehead region was observed as an observatory 'bad-weather' backup project on the James Clerk Maxwell Telescope (JCMT)[1] on Mauna Kea, Hawaii between 1993 and 1997 in CO 2-1 and ^{13}CO 2-1. All observations used the SIS heterodyne receiver RxA2 (Davies et al. 1992) with the Digital Autocorrelator Spectrometer (DAS)as a backend. The velocity resolution of DAS was 0.1 km s^{-1} and the velocity coverage ∼ 200 km s^{-1}. At 230 GHz the halfpower beamwidth (HPBW) of RxA2 was 21.″5 and the main beam efficiency, $\eta_{mb} = 0.68$. Except for a few early observations taken in total power raster mapping mode with a 20″ spacing all the observations were done in on-the-fly total power mode with integration times of 5 s per point and heavily oversampled (5″ spacing). For CO 2-1, we checked the calibration by taking a standard spectrum of OMC1 and/or the nominal center position of the map. For ^{13}CO(2-1), maps from night to night were designed to have significant overlap to ensure that we could maintain the relative calibration accuracy to within 5%. The scanning was done in both RA and Dec, and often repeated between different nights to improve the relative calibration and ensure that the rms level was approximately constant over the whole area mapped. Sandell et al. (1999) and Sandell et al. (2001) present some preliminary results from this project. **The velocity resolution (channel spacing) of the ^{12}CO 2-1 data cube is 0.2 km s^{-1}; the velocity resolution of the ^{13}CO 2-1 data cube is 0.1 km s^{-1}.**

All the data reduction was done manually using the Starlink package SPECX. Low order baselines were removed and occasionally standing wave ripple. Spectra were re-calibrated when necessary and coadded by weighting with rms noise. Really bad spectra were thrown out. The final CO 2-1 and ^{13}CO 2-1 maps have about 10,000 spectra each . In Jenness et al. (2015) and Jenness & Economou (2015) they tested the automated ORAC-DR pipeline by running it on the complete ^{13}CO(2-1) data set and compared it directly with the manually reduced data presented here. The automated pipeline does a good job were the data quality is reasonable, but for a data set like this, which contains data that have to be re-calibrated, a manual reduction is preferable.

The data cubes were converted into two-dimensional images presented in the Figures using a combination of software tools including the *Starlink Gaia* package, the *IRAF* package from NOAO and STScI, and *CASA* from NRAO and ALMA. Spectra were averaged over various spatial and spectral ranges using boxcar and Gaussian convolution in *IRAF* as well as *regions (reg) files* of various dimensions in *SAO Image ds9*. The image display tool, *SAO Image ds9*, was used to combine individual images into RGB color versions and to generate labels.

2.4. *NOAO*

The Hα image used here was obtained with the Mosaic 1 CCD and an 80Å narrowband filter centered at 6563Å. The image was made from a dithered set of five 600 second exposures acquired at the prime-focus of the Mayall 4-meter reflector on 30 October 1997 (MJD 50750) and reduced using the IRAF package MSCRED using standard procedures. The scale is 0.258″per pixel.

3. RESULTS

Figures 3 and 4 show [C$^+$] 157 μm channel maps of the Horsehead Nebula and its immediate surroundings. A three color scheme is used in which three adjacent ΔV = 0.96 km s^{-1} wide channels are shown in each panel in blue, green, and red, respectively. The central LSR radial velocities are shown in the colored numbers. This three-color radial velocity filter slides through the data cube in 1 km s^{-1} steps.

Figure 5 shows [C$^+$] spatial velocity diagrams along six east-to-west strips whose locations are indicated on the Hα narrow-band image shown in Figure 1; Three adjacent strips, separated by 0.008° (28.8″) in declination are shown in red, green, and blue. The left panel shows the [C$^+$] 157 μm line while the right panels show CO 3-2 emission along the same strips. **Figure 6 shows [C$^+$] along six north-south strip-maps indicated by solid (top) and dashed (bottom) lines in Figure 1 as indicated in the Figure 6 caption. The Right Ascensions are indicated by**

[1] The James Clerk Maxwell Telescope was operated on a joint basis between the United Kingdom Particle Physics and Astronomy Research Council (PPARC), the Netherlands Organization for the Advancement of Pure Research (ZWO), the Canadian National Research Council (NRC), and the University of Hawaii (UH).

the numbers in their respective colors. Figures 7 and 8 show pairs of $\Delta V = 0.25$ km s^{-1} wide CO 3-2 channels surrounding the velocity center of the $\Delta V = 1.0$ km s^{-1} wide [C$^+$] channels. (This scheme was use to better match the higher S/N CO 3-2 data to the lower S/N [C$^+$] channel images.) Figures 9 and 10 show comparisons between various radial velocity channels in [C$^+$], corresponding ^{12}CO 3-2 emission, and Hα. Figures 11 and 12 show comparisons between various radial velocity channels in [C$^+$], corresponding ^{13}CO 2-1 emission, and Hα. Figures 13 and 14 show eight east-west spatial velocity cuts through the Horsehead Nebula (top) and surrounding parts of the IC 434 ionization front (bottom) comparing the the [C$^+$] emission (green) with ^{12}CO 3-2 emission (red).

Figures 3 through 6 show that in the thin, <30″ wide PDR along the western rim of the dense Horsehead Nebula protrusion into IC 434, the [C$^+$] line reaches a peak value of 22 K near the location of the young stellar object IRAS 05383−0228 identified by Reipurth & Bouchet (1984). This region exhibits the narrowest linewidth in the entire mapped region in both CO 3-2 and [C$^+$] with ΔV(FWHM) $\sim$ 1.3 km s^{-1} (Fig. 6) . However, averaging the emission over a 30″ to 60″ diameter area shows that at the 1 K level, the [C$^+$] line has a width ΔV(FWHM) $\sim$ 3.5 km s^{-1} indicating some C$^+$ has been accelerated. The [C$^+$] emission from the Horsehead PDR and body is associated with the most blushifted portion of the mapped part of the Orion B cloud with the line peaking around $V_{LSR} \sim 10.4$ km s^{-1}. **Comparison of the CO 3-2 and [C$^+$] emission in Figure 13 shows that both species exhibit slightly broader linewidths and brighter emission in the thin Horesehead PDR along the western edge of the Horsehead then at positions to the east where the gas is shielded. Here, the [C$^+$] line is marginally broader than CO by about 0.3 to 0.5 km s^{-1}; both lines have the same central radial velocity within the measurement errors of $\sim$0.1 km s^{-1}. These features are best illustrated in Figure 13d which shows two prominent PDRs associated with narrow (< 1 km s^{-1} wide) CO lines, one associated with the Horsehead PDR at $V_{LSR} = 10.4$ km s^{-1} and R.A. = 85.22, and the other with a narrow-line component in the background at $V_{LSR} = 13$ km s^{-1}. at R.A. = 85.31 in Figure 13d.**

About $\sim$1′ east, between the Horsehead PDR and the 'neck' seen in CO 3-2 and dust continuum maps, there is a 1′ by 3′ north-south oriented region of dim [C$^+$] emission with a peak line brightness of $\sim$6 K at $V_{LSR} \approx 11.1$ km s^{-1} and ΔV(FWHM)$\sim$2.0 km s^{-1}, slightly redshifted by about 0.4 to 0.6 km s^{-1}, and broader than the emission from the Horsehead PDR. **This feature is labeled the 'Gap' in some of the figures.** Although this feature is seen as a hole in [C$^+$], it is filled with CO emission. It is likely that the [C$^+$] emission here is formed along the illuminated, back-side of the Horsehead protrusion.

Farther east, the [C$^+$] and CO 3-2 lines blend with emission from the Orion B cloud and west-facing IC 434 PDR and I-front. Both species exhibit broader linewidths ΔV(FWHM)$\sim$3.0 to 4.0 km s^{-1} and ΔV(1 K)$\sim$5.0 to 8.0 km s^{-1} with the peak emission and the overall line profile redshifted by about 0.5 to 3 km s^{-1} compared to the Horsehead PDR. While at the radial velocity of the Horsehead the [C$^+$] emission reaches a peak of $\sim$ 8 to 12 K, the line on the east side of the mapped field is often double-peaked with a brighter 13 to 16 K [C$^+$] component peaking at $V_{LSR} \approx 11.5$ to 12.5 km s^{-1}. This emission is likely associated with parts of the molecular cloud and PDR located in the background. **This emission can be clearly seen in Figures 13 between R.A. = 85.25 and 85.30.**

The north-south IC 434 I-front and PDR is clearly traced by corrugated, parallel ridges of [C$^+$] emission between $V_{LSR} \approx 8.0$ to 15 km s^{-1} with the line peaking between $V_{LSR} \approx 10.0$ to 12 km s^{-1}. Within $\sim$5′ of the I-front traced by the sharp edge of Hα emission, the peak [C$^+$] line strength reaches values between 15 and 25 K, about a factor of two higher than the peak line strength farther east in the Orion B cloud. Because this structure disappears behind the Horsehead in visual-wavelength images, it is clearly in the background.

Figures 7 and 8 show channel-by-channel comparisons of the optically thick ^{12}CO 3−2 and [C$^+$] 157 μm emission with similar angular resolution. Figures 9 and 10 show comparisons between Hα, [C$^+$] , and ^{12}CO 3−2 emission in various radial velocity channels. The north-south velocity gradient along the Horsehead noted by Hily-Blant et al. (2005) is evident in panels b), c), and d) in Figure 9.

Figures 11 and 12 show comparisons between the ^{13}CO 2−1 emission which mostly traces optically thin carbon monoxide, the [C$^+$] emission in corresponding channels, and Hα emission. The ^{13}CO emission in 0.1 km s^{-1} wide channels closest to the central radial velocity of the 0.96 km s^{-1} wide [C$^+$] 157 μm channels are used in this comparison because of the relatively lower signal-to-noise ratio of the [C$^+$] data.

The peak brightness of the CO 3-2 line in the Horsehead Nebula, integrated over the area of the stem, but excluding the Nose and Mane is about T_A^*(3-2)$\approx$ 6 K. In contrast, the CO 2-1 line in the

same region has a peak of T_A^*(2-1) ≈ 15 K and ^{13}CO 2-1 has a peak temperature $^{13}T_A^*$(2-1)≈ 7 K. In the Horsehead PDR, the peak intensities are T_A^*(3-2)≈ 11K; T_A^*(2-1) ≈ 22 K; $^{13}T_A^*$(2-1) ≈ 11 K.

Several patterns are evident in these figures:

1) The Horsehead 'neck', 'mane', and the anvil-shaped 'western-ridge' (Pound et al. 2003 designations) are filled with CO emission with T_{CO}(2-1) ∼15 to 23 K and T_{CO}(3-2) ∼13 to 32 K with the peak temperatures occurring along the western rim PDR close to the location of IRAS 05383-0228. Bright [C$^+$] emission is concentrated in a narrow north-south oriented, ∼0.03 pc wide ridge along the Horsehead's western rim. The [C$^+$] emission reaches peak brightness temperatures of T(C$^+$) ∼22 K near IRAS 05383-0228 with T(C$^+$) ∼15 K near the base of the Horsehead in the 'neck'. Radial velocity differences between the CO and [C$^+$] emission amount to less than 0.5 km s^{-1}. Most [C$^+$] emission in the mapped region is redshifted with respect to the Horsehead Nebula.

2) Bright, lumpy filaments of [C$^+$] emission with a width of ∼0.1 pc trace the eastern side of the IC 434 I-front seen in Hα emission. These features appear to be edge-on sheets along the interface between the background portion of western edge of the Orion B cloud and I-front. The [C$^+$] emission reaches peak brightness temperatures of T(C$^+$) ∼15 to 20 K along the ridge but declines by about a factor of two to the east. Clumpy CO emission extends to within 0.05 pc of the [C$^+$] edge along the top one-third of the mapped field. T_{CO}(2-1) ∼15 to 23 K and T_{CO}(3-2) ∼5 to 12 K in this region The emission in this region is broad with ΔV(FWHM) ∼4 to 5 km s^{-1} and extends to at least V_{LSR} = 15 km s^{-1}.

3) A 2′ diameter elliptical ring of [C$^+$] emission around V_{LSR} ∼13 to 14 km s^{-1} (panels g and h in Figure 8; f an g in Figure 10; g in Figure 12) can be seen around Declination −2° 22′ along the western rim of the PDR. The northern rim of this ring exhibits the highest brightness temperature in [C$^+$] along the IC 434 PDR, ∼25 K with ΔV(1 km s^{-1}) ∼8 km s^{-1}. A tongue of CO emission pierces the ring. However, this molecular feature had a radial velocity about 1 km s^{-1} lower (blushifted) than associated [C$^+$] ring.

4) A 5′ (0.6 pc diameter) 'bay' between the [C$^+$] ring and associated CO protrusion and the Horsehead is devoid of CO emission. However, this region is filled with [C$^+$] having peak brightness temperatures of 10 to 15 K and line-widths of order 5 km s^{-1}. Unlike in the Horsehead region and in the northern part of the field where the [C$^+$] dominated PDR is less than 0.05 pc thick, the PDR in the bay is ∼0.5 pc wide in projection. Although most of the [C$^+$] emission over the mapped field is single peaked, the [C$^+$] between the center of the bay and the north rim of the Horsehead at its base is double-peaked with a peak separation of about 2 to 2.5 km s^{-1} (Fig 6, top panel). There is no CO emission along the line of sight to most of the bay. Thus, this extensive feature is not a face-on ionization front. Deep visual and near-IR images show that the 'bay' is a cavity within the molecular cloud which contains several highly reddened stars. Stars of spectral type late-B, A, or early F within the 'bay' may produce sufficient FUV radiation to produce this structure.

5) The brightest [C$^+$] emission is found within one or two beam-widths (15″ to 30″) of the I-front traced by Hα and diminishes in intensity by at least a factor of two towards the east. The CO emission in both the 2-1 and 3-2 transitions remain relatively constant as one moves from the I-front and PDR to the east into the cloud interior.

6) The ionized region west of the IC 434 I-front exhibits weak 0.5 to 1 K and broad, ΔV ∼5 km s^{-1}, [C$^+$] and dim <1 K CO 3-2 emission. This emission **either arises from inside the HII regions where electron impacts can excite the [C$^+$] line, or is associated with low-column density (< 10^{20} cm^{-2}) veils of atomic or molecular gas located either in front or behind the IC 434 HII region. As shown by (Goldsmith et al. 2012), the critical density for exciting the [C$^+$] transition at T$_e$ = 8,000 K in about n_e ≈ 44 cm^{-3}. As discussed below, the electron density in the HII region interior is likely to be around 30 cm^{-3} which is sufficient to excite the 157 μm line.**

7) The west-facing edges of clumps and molecular protrusions located east of the IC 434 I-front are rimmed by [C$^+$] emission. The radial velocity differences between the CO and [C$^+$] emission are less than 1 km s^{-1}. **Because the Horsehead Nebulae emission has a very narrow linewidth, a small radial velocity difference between the ^{13}CO 2-1 and [C$^+$] are most apparent there. Figures 13 and 14 show the ^{12}CO 3-2 emission in red, superimposed on the [C$^+$] emission in green along east-west cuts through the IC-434 ionization front.** Most [C$^+$] rims have widths of 15″ to 30″ and some may be unresolved in the SOFIA 15″ beam.

4. DISCUSSION

4.1. *I-front Driven D-type Shocks, Accelerations, and Compressions in the PDR*

The Lyman continuum luminosity of an 09.5 star such as σ-Ori is about Q = 1.6×10^{48} EUV photons s^{-1} (Sternberg et al. 2003). For a uniform density Strömgren sphere with a radius of 4 pc (the projected distance between the Horsehead Nebula and σ-Ori), the mean electron density is, in the absence of internal attenuation by dust, $n_e \approx 28$ cm^{-3}. For a dense, spherical cloud with a hydrogen number density much larger than this value, the electron density at the base of the I-front is set by recombination rate between the cloud surface and the star in the roughly spherically diverging, ionized, photo-ablation flow from the cloud. For a cloud with a radius $R_c \sim 8 \times 10^{17}$ cm, comparable to the semi-diameter of the Horsehead nebula, the electron density at the base of an ionization front that wraps around it is expected to satisfy $Q/4\pi D^2 = n_e^2 \alpha_B R_c/3$ where $\alpha_B \approx 2.6 \times 10^{-13}$ cm^{-6} s^{-1} is the case-B recombination coefficient for hydrogen at about $T = 10^4$ K, and $D = 4$ pc is the distance from the ionizing source. For these parameters, $n_e \sim$112 cm^{-3}. The sound speed in the fully ionized gas is expected to be around $c_{II} \approx 10$ km s^{-1}. The D-type shock powered by the ionization front is expected to move with a velocity

$$V_D = c_{II}\Big[\frac{\rho_{II}}{\rho(H_2)(1-\rho_{II}/4\rho(H_2))}\Big]^{1/2} \approx c_{II}\Big[\frac{\rho_{II}}{\rho(H_2)}\Big]^{1/2}$$

were $\rho(H_2)$ is the molecular cloud density and $\rho_{II} = \mu m_H n_e$ is the fully ionized plasma density. For a neutral H_2 density n(H_2) = 5×10^3 cm^{-3} (Pound et al. 2003), the D-type shock powered by the ionization front is expected to move with a velocity $V_D \sim 1.1$ to 0.5 km s^{-1} for the Strömgren sphere and cloud geometries respectively. Given that σ-Ori is located 4 pc in projection to the west of the IC 434 I-front suggests that the radial velocities will be lower by a factor $1/sin(\theta) \sim$2 to 3 where θ is the angle of illumination with respect to the plane of the sky.

In the limit that the pre-shock cloud pressure is given by thermal pressure (e.g. magnetic fields are negligible), the density of the post-shock layer is given by $\rho_{ps} = P_{II}/c_I^2$. The density of the post-shock layer depends only on the adjacent HII region pressure and sound speed in the pre-shock cloud and is independent of the cloud pre-shock density. For a sound speed $c_I = 0.24$ km s^{-1}, appropriate for 20 K molecular gas and $n_e = 25$ to 110 cm^{-3}, the post-shock density of 20 K molecular gas is $n(H_2) \approx 2$ to 9×10^4 cm^{-3}. These post-shock densities bracket the values found for the Horsehead PDR.

The [C$^+$] emission mostly forms in the PDR where N(H) $\leq$ 1 to 4×10^{21} cm^{-2} were CO is dissociated into CI and ionized to form CII by FUV, and H_2 transitions into HI (Pellegrini et al. 2009; Sternberg et al. 2014). Nearly edge-on I-fonts such as IC 434 are good environments in which to separate organized, large-scale motions from chaotic motions and turbulence. If UV radiation generates significant turbulence, then the line-width and line-of-sight velocity dispersion will be largest near the I-front and decrease with increasing distance into the cloud. If, on the other hand UV-induced turbulence generation is low, there will be no correlation between velocity dispersion and distance into the cloud from the I-front.

The line-widths of the Horsehead PDR are nowhere less than about 1 km s^{-1} at least a factor of two larger than the spectral resolution of [C$^+$] observations, and a factor of four larger than the sound-speed in the cold ~20 K molecular gas, even in the nearly face-on PDRs in the back side of the protrusion seen through the CO-rich Horsehead interior. (The native spectral resolution is much higher; data were re-sampled to a resolution of 0.2 km s^{-1}; thus a 1 km s^{-1} line is well resolved). If this broadening is due to thermal motion only, the sound speed in in the bulk of the [C$^+$] emitting layer must be >300 K. However, it is more likely that this linewidth reflects a combination of acceleration in the PDR, or the variation of shock speeds created by unresolved density structure.

4.2. *C$^+$ Column Densities*

Goldsmith et al. (2012) presented an analysis of the excitation and radiative transfer in [C$^+$]. We estimate column densities from the SOFIA [C$^+$] data using the formulae given in Langer et al. (2017) which is based of the Goldsmith et al. (2012) work. The column density of C$^+$is given by

$$N(C^+) = 2.92 \times 10^{15}\Big[1 + \frac{e^{\frac{\Delta E}{kT}}}{2}\Big(1 + \frac{n_{crit}}{n}\Big)\Big] I(C^+) \quad cm^{-2}$$

where $I(C^+) = \int T_{CII}(V)dV$ is in K km s^{-1} and n is the volume number density of the dominant collision partner (electrons, H atoms, or H_2 molecules), $\Delta E/k = 91.2$ K, and T is the temperature of the region. The [C$^+$] line can be collisional lyexcited by electron impacts in the HII region (T ~ 8,000 K), in the mostly atomic and warm (T ~100 to 6,000 K) PDR by collisions with hydrogen and helium atoms, or in the molecular PDR where hydrogen is mostly in the form of H_2 but CO has been **mostly** dissociated by FUV into C and O and **some** C has been ionized (T ~ 20 to

100 K). The critical densities (n_{crit}) for these three situations are given as a function of temperature in Goldsmith et al. (2012) Table 2.

Table 1 gives some representative [C$^+$] line parameters such as the peak line temperature and width, the integrated line intensity, and derived line-of-sight column densities as functions of gas density and temperature **in circular regions with a radii of integration listed in Table 1 and shown in Figure 15.** It is assumed that most of the [C$^+$] emission originates in the predominantly atomic layer **where hydrogen in neutral, but all carbon is in C$^+$,** and that the FUV penetrates to a depth corresponding to a hydrogen column or order N(H) $\sim 10^{21}$ cm^{-2}. The very thin, 0.05 to 0.1 pc PDR along the western rim of the Horsehead combined with this FUV penetration depth implies a density n(H)>3,000 cm^{-3}. In contrast, the broad 0.5 pc PDR in the 'bay' region implies an order of magnitude lower density.

The photoionized interior of the IC-434 HII region also emits in the [C$^+$] line. Assuming a plasma (electron) temperature of T = 8,000 K and a mean electron density n_e = 28 cm^{-3} (estimated above if the HII region is a uniform-density Strömgren sphere) implies that that the column density of H in the HII region west of the I-front is about $2.4 \pm 1 \times 10^{20}$ cm^{-3} based on the above formula. This is close to what is expected from N(HII) = n$_e$ L = 3.5×10^{20} cm^{-3}. The [C$^+$] fluxes imply that north of the Horsehead, where Hα is brighter, N(HII) $\approx 3 \times 10^{20}$ cm^{-3} while south of the Horsehead, where Hα is dimmer, N(HII) $\approx 1.7 \times 10^{20}$ cm^{-3} under these assumptions. The lower-values derived from the [C$^+$] line imply that either the mean electron density in the HII region is less than 28 cm^{-3}, and/or that the effective path length through the HII region is shorter than 4 pc.

Pressure equilibrium between the IC 434 HII region and the PDR constrains the product of temperature and density in the predominantly atomic layer. For electron densities in the range n_e = 30 to 100 cm^{-3} in the HII region, $P/k \approx n_{PDR} T_{PDR} = 2.4 - 8.0 \times 10^5$ cm^{-3}K for plasma temperatures of 8,000 K. Thus, $n_{PDR} \approx 2.4 - 8.0 \times 10^5 / T_3$ where T_3 is the PDR temperatrue in units of 10^3 K. Table 1 give the derived line-of-sight column densities of H as for a range of temperatures and densities assuming a C$^+$ abundance of 2×10^{-4} with respect to atomic hydrogen (Nieva & Przybilla 2008) and optically thin [C$^+$] emission.

Recent unpublished SOFIA/upGREAT measurements of [^{13}C$^+$] indicate that most of the [^{12}C$^+$] emission in and near the Horsehead Nebula region has a low optical depth. The highest value, $\tau \sim$1.5 occurs where the [C$^+$] line has the largest peak temperature (Guevara 2017). However, Pabst et al. (2017) detected the [^{13}C$^+$] in the SOFIA data by averaging spectra over many beam-widths. Following the work of Pabst et al. (2017), we re-analyzed the [C$^+$] data cube by averaging spectra over regions varying in size and shape from 15″ to over 600″. The only unambiguous detection of the [^{13}C$^+$] F = 2−1 line occurs in the Horsehead PDR in a 30″ by 150″ at V$_{LSR}$ $\sim$ 22 km s^{-1} in our data (in which radial velocities are referenced to the [^{12}C$^+$] line). The [^{13}C$^+$] line has an intensity about 30 times lower than the [^{12}C$^+$] line. However, the diffuse and faint [^{12}C$^+$] emission from the IC 434 HII region West of the Horsehead has a broad linewidth extending to at least this LSR radial velocity and may contribute to the emission around V$_{LSR}$ $\sim$ 22 km s^{-1} in the Horesehead PDR. We conclude that while the [C$^+$] emission is optically thin over most of the mapped area, it may have an optical depth of a few in the Horsehead PDR, resulting in slightly higher column densities than implied by the estimates in Table 1.

Along the Horsehead PDR, **[C$^+$] -based N(H)** column densities of order 1 to 10×10^{21} cm^{-2} are derived. This is consistent with a PDR with a penetration depth of $\sim 10^{21}$ cm^{-2} seen close to edge-on. These parameters suggest that the 'Gap' in the Horsehead [C$^+$] emission corresponds to a region where the C$^+$ layer is seen close to face-on on the backside of the protrusion into the IC 434 HII region (see Figure 3c).

The 'bay' region consists of an unusually thick, ∼0.5 pc PDR layer. If the penetration depth is $\sim 10^{21}$ cm^{-2}, the density must be an order of magnitude lower than in the Horsehead PDR. Pressure balance with the HII region implies an order of magnitude higher temperature in the 'bay' than in the Horsehead PDR. The ∼70 K km s^{-1} integrated intensity of [C$^+$] translates into a column density ranging from $6 - 20 \times 10^{21}$ cm^{-2}, suggesting that our line-of-sight lies close to the tangent to the PDR (e.g. it is seen edge-on). The thinner, 0.1 to 0.2 pc wide PDR along the northern part of the mapped field also has high column intensities, consistent with and edge-on geometry.

The bulk of the PDR behind the IC 434 I-front is redshifted compared to the Horsehead. Given that the Horsehead protrusion **is seen in silhouette in Hα, it must be slightly closer to us than σ-Ori and primarily illuminated along its back side.** This velocity difference **and location of the Horsehead in the foreground** is consistent

with a compressed layer along the western side of Orion B expanding away from σ-Ori, mostly at right angles to our line of sight as shown in Figure 2 relative to the un-impacted parts of the Orion B molecular cloud.

Ochsendorf et al. (2014) proposed that σ-Ori is moving *towards* the northeast and Orion B with a proper motion of about 15 km s^{-1} (position angle 49.9°). If this motion corresponds to the relative motion of the star and the cloud, then the radiation field impinging on the IC 434 HII region has been increasing in time over the last several Myr. It is likely that the combination of FUV photo-ablation, EUV photo-ionization, and radiation pressure have accelerated the western edge of the Orion B cloud to a velocity ∼1 to 3 km s^{-1}. The plasma density near relatively straight sections of the I-front is set by the Strömgren condition to be around 10 to 40 cm^{-3} but may be several times higher around dense protrusions surrounded by convex I-fronts supporting divergent flows as discussed above. Thus, the velocity and penetration depth of the resulting D-type shock fronts depend on the cloud density with faster shocks moving into lower density portions of the cloud.

The order-of-magnitude increase in the thickness of the C$^+$ layer in the 'bay' PDR compared with the thin PDR wrapping around the Horsehead must be a consequence of the curvature of the D-type shocks, PDRs, and I-fronts. Convex regions such as around the Horsehead result in thin C$^+$ layers while concave regions produce thick C$^+$ layers. The 'bay' region may have been carved out where the I-front encountered lower densities while the Horsehead may be a region where the I-front encountered higher densities. Since the 'bay' appears to be surrounded by denser protrusions which have retarded the advancing I-fronts to both the north and south, it is possible that converging atomic flows from the PDRs at the surfaces of these protrusions account for the 0.5 pc depth of the C$^+$ layer here (see Fig. 2).

Because faster shocks moving into lower-density gas are more compressive than the slower shocks moving into denser gas, the compressed post-shock layer between the PDR and the D-type shock is expected to have a relatively uniform density even though it is moving into a highly structured medium with large density variations. Thus, the PDR layer may be more uniform than the cloud into which it moves. This feature can explain the relatively uniform peak brightness of the [C$^+$] emission in the PDR, and the Hα emission in the IC434 I-front.

4.3. *Origin of the Horsehead and dense gas layer along the IC 434 I-front*

IC 434 ionized by σ-Ori is **one of the youngest HII regions to form in the 10 to 15 Myr old Orion OB1 association which is** centered west of the Orion B cloud (Bally 2008). If the Orion B cloud initially extended 4 to 8 pc to the west where σ-Ori and its associated cluster formed 3 to 4 Myr ago, and if it had a uniform mean density n(H$_2$) $\sim 3 \times 10^3$ cm^{-3} then the amount of mass displaced by expansion of the HII region created by σ-Ori would have been at least 10^4 M$_\odot$. At a mean electron density of about 28 cm^{-3}, the current mass in this ∼4 pc radius bubble of plasma is only about ∼100 M$_\odot$. Thus, most of the mass displaced by the HII region must be in a shell compressed by a D-type shock ahead of the advancing I-front. Assuming a spherical shell, division of the displaced mass minus the HII region mass by the shell area gives the shell column density. For the above parameters, this results in an upper bound of $N(H_2) \approx 4 \times 10^{21}$ cm^{-2} for the column density of the shell by the expansion of the IC 434 HII region into a hypothetically uniform density medium. But, if a 'champagne flow' expelled most of this mass to the west, the shell column density would be lower. **However, feedback from older generations of massive stars in Orion OB1 likely also impacted the Orion B cloud. Thus, the amount of material pushed towards the east and swept-up in a dense layer may have a larger column density than what σ-Ori could create by itself.**

As discussed above, post-shock density behind a D-type shock, in the isothermal limit, is relatively insensitive to the density structure of the cloud into which the shock is moving. **Ignoring internal turbulent support,** the density is expected to be $n(H_2) \sim few \times 10^4$ cm^{-3}. Dividing the shell column density estimated above by this density implies a very thin shell with a thickness of only ∼0.05 pc, comparable to the thickness of the PDR layers observed in [C$^+$]. We conclude that the structures encountered by the expansion of the IC 434 I-front must be pre-existing density structures in the Orion B cloud.

The Horshead nebula has a distinctive 'anvil' shape consisting of a 2′ wide stem of dense molecular gas traced by CO surrounded along its western end by a 4′ wide sheet of dense CO and dust consisting of the Mane and Nose. This sheet wraps around the stem to produce a bow-shaped structure deflected towards the east. The Horeshead PDR traces the western rim of this feature. Evidently, the thermal pressure of the heated PDR, combined with back-pressure exerted by the westward expansion of the photo-ionized plasma flowing away from the PDR and feeding the IC 434 HII region has accelerated the Nose and Mane towards the east. The eastern tip of the Horse's Nose and the Mane have been displaced to the east by about 3′ or 0.3 to 0.4 pc with respect to the brightest part of the Horsehead

PDR near the YSO B33-1 (Reipurth & Bouchet 1984). If the Horsehead has been exposed for ∼1 Myr, this implies a velocity difference of ∼ 0.3 to 0.4 km s^{-1} between the eastern parts to the Mane, Nose, and the western edge near B33-1, comparable to the ∼0.5 km s^{-1} north-south velocity gradient seen in CO. However, most of the flow in the anvil is likely to be along the plane of the sky. Indeed no clear east-west velocity gradient is seen in either CO or [C$^+$].

Wide field studies of the ∼ 10^5 $M_\odot$ Orion B molecular cloud show that most recent (<1 to 3 Myr) star formation has occurred along its Western rim. Older episodes of star formation created the a, b, and c subgroups of the Orion OB1 association over a time span extending back at least 12 Myr. These older than sub-groups of OB stars formed to the west of Orion B. The OB stars have completely destroyed the molecular gas from which they formed, creating the Orion-Eridanus super-bubble (Bally 2008; Pon et al. 2014, 2016; Ochsendorf et al. 2015). Over ∼10 to 15 Myr, the combined effects of expanding HII regions, the shocks powered by stellar wind bubbles, and multiple supernovae would have destroyed the parent clouds and eroded low-density gas between their location and Orion B. Some of the material could have been swept into dense shells along the western rim of the Orion B cloud, producing a several pasec-wide dense layer where star formation has been igniting over the last several Myr. This activity could have produced the clumpy structure now revealed as the Horsehead and adjacent protrusions of dense gas.

Tremblin et al. (2012a,b) present numerical models of 'elephant trunk' or pillar formation in advancing shock systems powered by expanding HII regions. They argue that small density variations which lead to I-front curvature forms dense pillars as the I-fronts converge. Such a model applied to a several Myr evolution of the I-fronts acting on the Western rim of the Orion B cloud can lead to structures such as the Horsehead Nebula.

Finally, the magnetic field in the mapped portion of Orion B runs mostly north-south (Zaritsky et al. 1987). Such a field orientation suggest that the Western rim of Orion B is part of a swept-up shell in which compression has partially aligned the magnetic field with I-front. This field geometry may suppress compression and inhibit the gas flows at right-angles to the field and away from the PDR.

4.4. *Comparison with Pabst et al. (2017)*

We briefly compare our findings with Pabst et al. (2017). While this study concentrates on the kinematics of the [C$^+$] emission and its morphological relation to other tracers such as CO and Hα and dust emission, the Pabst et al. (2017) study models the PDR physics. Both studies find that the bright [C$^+$] layers in the Horsehead PDR are thin (L <0.05 pc) with an estimated n(H$_2$) = 2 − 6×10^4 cm^{-3}; Pabst et al. (2017) found a value of 4×10^4 cm^{-3}. Both studies find that the contributions of the extended HII region west of IC 434 to the [C$^+$] emission is small and produces a broad but faint emission line. Assuming that the HII region has a line-of-sight depth of 1 pc, Pabst et al. (2017) estimate an electron density of 95 cm^{-3}. Assuming a spherical HII region with a radius of 4 pc, we find a mean density of 28 cm^{-3}. Assuming a spherically diverging flow of plasma from the Horsehead protrusion with a mean ionization front radius of 8×10^{17} cm, we estimated an electron density of 115 cm^{-3} at the base of the I-front where the impinging ionizing radiation field shines on the cloud at right angles.

Based on the peak brightness temperature of the [C$^+$] emission and the expected gas temperature of PDR, we conclude that the [C$^+$] emission is mostly optically thin. Pabst et al. (2017) averaged the spectra over large areas to detect the faint [^{13}C$^+$] emission line and use the intensity of this line to estimate [C$^+$] optical depths of around 1 to 5. Thus our column density estimates tend to be a bit lower. However, Guevara (2017) used new [^{13}C$^+$] observations (from SOFIA Cycle 4 program 05_0057) and found that the highest optical depth was 1.5 at the location of the brightest [C$^+$] peak.

We searched the [C$^+$] data cube for the [^{13}C$^+$] F=2-1 and F=1-1 lines by averaging spectra using *SAO Image ds9* region files with a range of sizes and displaying the resulting spectra. The strongest [^{13}C$^+$] F=2-1 was found along the narrow, north-south ridge comprising the ionization front at the west rim of the Horsehead. The intensity ratio here is about 40±10, indicating that the optical depth of [C$^+$] is around 2. However, along the main ionization front at the western rim of the Orion B cloud where the peak brightness of [C$^+$] reaches 25 K, the [^{13}C$^+$] F=2-1 is not detected.

5. CONCLUSIONS

SOFIA [C$^+$] observations of the Horsehead Nebula regions are combined with ground-based Hα and CO 2-1 and 3-2 observations to study the morphology and kinematics of the I-fronts, atomic PDR, and D-type shocks. Because the

Horsehead is seen in silhouette against the background IC 434 HII region mostly ionized by σ-Ori, it must be located in the foreground part of the Orion B cloud. Because the Horsehead is associated with the most blueshifted CO and [C^+] emission, we conclude that was produced by a dense clump in a parsec-scale dense layer of swept-up gas along the western rim of the Orion B cloud powered by previous generations of OB stars in the 3 to 15 Myr old sub-goups a, b, and c of the Orion OB1 association located north and west of the Horsehead.

We thank the up-GREAT team and the SOFIA Project for making the [C^+] data available. The observations were taken as part of the director's discretionary time under the direction of Dr. Erick Young to demonstrate the power and speed of the upGREAT THz heterodyne camera.

The NASA/DLR Stratospheric Observatory for Infrared Astronomy (SOFIA) is jointly operated by the Universities Space Research Association, Inc. (USRA), under NASA contract NAS2-97001, and the Deutsches SOFIA Institut (DSI) under DLR contract 50 OK 0901 to the University of Stuttgart.

GREAT is a development by the MPI für Radioastronomie (Principal Investigator: R. Güsten) and the KOSMA/ Universität zu Köln, in cooperation with the MPI für Sonnensystemforschung and the DLR Institut für Planetenforschung.

CLASS is part of the Grenoble Image and Line Data Analysis Software (GILDAS), which is provided and actively developed by IRAM, and is available at http://www.iram.fr/IRAMFR/GILDAS.

The APEX observations were made possible through observing time granted by the European Southern Observatory (ESO) proposal numbers E-094.C-0935, O-094.F-9343.

This work has made use of data from the European Space Agency (ESA) mission *Gaia* (https://www.cosmos.esa.int/gaia), processed by the *Gaia* Data Processing and Analysis Consortium (DPAC, https://www.cosmos.esa.int/web/gaia/dpac/consortium). Funding for the DPAC has been provided by national institutions, in particular the institutions participating in the *Gaia* Multilateral Agreement.

Facilities: SOFIA 2.5-meter, APEX 12-meter, JCMT 15-meter, NOAO Mayall 4-meter telescopes

Software: Starlink Gaia, CASA, IRAF / PyRAF, CLASS, Anaconda Pyton, SAO Image ds9

REFERENCES

Abergel, A., Teyssier, D., Bernard, J. P., et al. 2003, A&A, 410, 577

Andree-Labsch, S., Ossenkopf-Okada, V., & Röllig, M. 2017, A&A, 598, A2

Bally, J. 2008, Handbook of Star Forming Regions, Volume I, 4, 459

Bally, J., Langer, W. D., Stark, A. A., & Wilson, R. W. 1987, ApJL, 312, L45

Bertoldi, F., & Draine, B. T. 1996, ApJ, 458, 222

Bowler, B. P., Waller, W. H., Megeath, S. T., Patten, B. M., & Tamura, M. 2009, AJ, 137, 3685

Davies, S. R., Cunningham, C. T., Little, L. T., & Matheson, D. N. 1992, Int. J. Infrared Millimeter Waves, 13, 1827

Elmegreen, B. G., & Lada, C. J. 1977, ApJ, 214, 725

Gaia Collaboration, Brown, A. G. A., Vallenari, A., et al. 2016, A&A, 595, A2

Garcia-Segura, G., & Franco, J. 1996, ApJ, 469, 171

Goicoechea, J. R., Pety, J., Gerin, M., Hily-Blant, P., & Le Bourlot, J. 2009, A&A, 498, 771

Goicoechea, J. R., Pety, J., Cuadrado, S., et al. 2016, Nature, 537, 207

Goldsmith, P. F., Langer, W. D., Pineda, J. L., & Velusamy, T. 2012, ApJS, 203, 13

Gratier, P., Pety, J., Guzmán, V., et al. 2013, A&A, 557, A101

Guevara, C. 2017, PhD Thesis, University of Cologne: Private communication

Guzmán, V. V., Pety, J., Goicoechea, J. R., et al. 2015, ApJL, 800, L33

Guzmán, V. V., Goicoechea, J. R., Pety, J., et al. 2013, A&A, 560, A73

Guzmán, V., Roueff, E., Gauss, J., et al. 2012, A&A, 548, A94

Guzmán, V., Pety, J., Gratier, P., et al. 2012, A&A, 543, L1

Guzmán, V., Pety, J., Goicoechea, J. R., Gerin, M., & Roueff, E. 2011, A&A, 534, A49

Habart, E., Abergel, A., Boulanger, F., et al. 2011, A&A, 527, A122

Hily-Blant, P., Teyssier, D., Philipp, S., & Güsten, R. 2005, A&A, 440, 909

Hollenbach, D. J., & Tielens, A. G. G. M. 1999, Reviews of Modern Physics, 71, 173

Hosokawa, T., & Inutsuka, S.-i. 2006, ApJL, 648, L131

Hosokawa, T., & Inutsuka, S.-i. 2006, ApJ, 646, 240

Kloosterman, J., Cottam, T., Swift, B., et al. 2012, Proc. SPIE, 8452, 845204

Kounkel, M., Hartmann, L., Loinard, L., et al. 2017, ApJ, 834, 142

Jenness, T., Currie, M. J., Tilanus, R. P. J., et al. 2015, MNRAS, 453, 73

Jenness, T., & Economou, F. 2015, Astronomy and Computing, 9, 40

Lada, E. A., Bally, J., & Stark, A. A. 1991, ApJ, 368, 432

Langer, W. D., Velusamy, T., Morris, M. R., Goldsmith, P. F., & Pineda, J. L. 2017, A&A, 599, A136

Megeath, S. T., Gutermuth, R., Muzerolle, J., et al. 2012, AJ, 144, 192

Megeath, S. T., Gutermuth, R., Muzerolle, J., et al. 2016, AJ, 151, 5

Mookerjea, B., Sandell, G., Jarrett, T. H., & McMullin, J. P. å, 507, 1485

Nieva, M. F., & Przybilla, N. 2008, A&A, 481, 199

Ochsendorf, B. B., Brown, A. G. A., Bally, J., & Tielens, A. G. G. M. 2015, ApJ, 808, 111

Ochsendorf, B. B., Cox, N. L. J., Krijt, S., et al. 2014, A&A, 563, A65

Orkisz, J. H., Pety, J., Gerin, M., et al. 2017, A&A, 599, A99

Pabst, C. H. M., Goicoechea, J. R., Teyssier, D., et al. 2017, arXiv:1707.05976

Pellegrini, E. W., Baldwin, J. A., Ferland, G. J., Shaw, G., & Heathcote, S. 2009, ApJ, 693, 285

Pérez-Beaupuits, J. P., Wiesemeyer, H., Ossenkopf, V., et al. 2012, A&A, 542, L13

Pety, J., Gratier, P., Guzmán, V., et al. 2012, A&A, 548, A68

Pety, J., Guzmán, V. V., Orkisz, J. H., et al. 2017, A&A, 599, A98

Pon, A., Ochsendorf, B. B., Alves, J., et al. 2016, ApJ, 827, 42

Pon, A., Johnstone, D., Bally, J., & Heiles, C. 2014, MNRAS, 444, 3657

Pound, M. W., Reipurth, B., & Bally, J. 2003, AJ, 125, 2108

Reipurth, B., & Bouchet, P. 1984, A&A, 137, L1

Risacher, C., Güsten, R., & Stutzki, J., et al. 2016, A&A, 595, A34

Sandell, G., Jenness, T., McMullin, J. P., & Shah, R. Y. 2001, Bulletin of the American Astronomical Society, 34, 156.01

Sandell, G., Avery, L. W., Baas, F., et al. 1999, ApJ, 519, 236

Sternberg, A., Hoffmann, T. L., & Pauldrach, A. W. A. 2003, ApJ, 599, 1333

Sternberg, A., Le Petit, F., Roueff, E., & Le Bourlot, J. 2014, ApJ, 790, 10

Tielens, A. G. G. M., & Hollenbach, D. 1985, ApJ, 291, 722

Tremblin, P., Audit, E., Minier, V., Schmidt, W., & Schneider, N. 2012, A&A, 546, A33

Tremblin, P., Audit, E., Minier, V., & Schneider, N. 2012, A&A, 538, A31

Zaritsky, D., Shaya, E. J., Tytler, D., Scoville, N. Z., & Sargent, A. I. 1987, AJ, 93, 1514

Zhou, S., Jaffe, D. T., Howe, J. E., et al. 1993, ApJ, 419, 190

Table 1. Representative [C$^+$] Intensities, Temperatures, and Column Densities in the PDR

R.A. 5^h	Dec. -2°	Radius ($''$)	T_{gas}[a] (K)	n (cm^{-3})	ΔV (km s^{-1})	$T_{peak}(C^+)$ $T_{peak}(C^+)$	T_A^* dV (K km s^{-1})	N(H) (cm^{-2})	Comments
40 22	27 01	15	500	3000	1.3	22	31.8	9.7×10^{20}	Horsehead PDR
”	”	”	500	1000	”	”	”	1.4×10^{21}	Horsehead PDR
”	”	”	500	300	”	”	”	3.0×10^{21}	Horsehead PDR
”	”	”	500	100	”	”	”	7.4×10^{21}	Horsehead PDR
”	”	”	100	3000	”	”	”	1.5×10^{21}	Horsehead PDR
”	”	”	100	1000	”	”	”	2.4×10^{21}	Horsehead PDR
”	”	”	100	300	”	”	”	5.6×10^{21}	Horsehead PDR
”	”	”	100	100	”	”	”	1.5×10^{22}	Horsehead PDR
40 55.2	28 41	7.5	500	3000	1.9	13	30.0	9.1×10^{20}	Mane
”	”	”	500	1000	”	”	”	1.3×10^{21}	Mane
”	”	”	500	300	”	”	”	2.8×10^{21}	Mane
”	”	”	500	100	”	”	”	7.0×10^{21}	Mane
”	”	”	100	3000	”	”	”	1.4×10^{21}	Mane
”	”	”	100	1000	”	”	”	2.3×10^{21}	Mane
”	”	”	100	300	”	”	”	5.3×10^{21}	Mane
”	”	”	100	100	”	”	”	1.4×10^{22}	Mane
40 57.4	25 34	15	100	1000	1.2	11	19.1	1.5×10^{21}	Nose
40 58.7	26 46	15	100	1000	1.0	5	15.4	1.2×10^{21}	Gap
41 05.8	23 03	30	100	1000	3.5	18	74.3	5.7×10^{21}	Bay
40 59.6	20 55	15	100	1000	4.5	23	108.5	8.3×10^{21}	[C$^+$] peak
40 59.1	18 40	15	100	1000	3.0	12	11.5	8.7×10^{20}	North

[a]Estimated from the ^{12}CO 2−1 transition.

NOTE—The column density estimates assume that most of the [C$^+$] emission forms in the atomic layer by impacts with hydrogen, unless otherwise noted. A C$^+$ abundance of 2×10^{-4} relative to H, implying that in the [C$^+$] emission region all carbon is in the form of C$^+$ is assumed (Nieva & Przybilla 2008). In the absence of a direct measure of gas temperature in the PDR, we use a range of plausible values ranging from 100 to 3,000 K for the first two entries. The dependences on T and n for these regions can be extrapolated to the remaining entries.

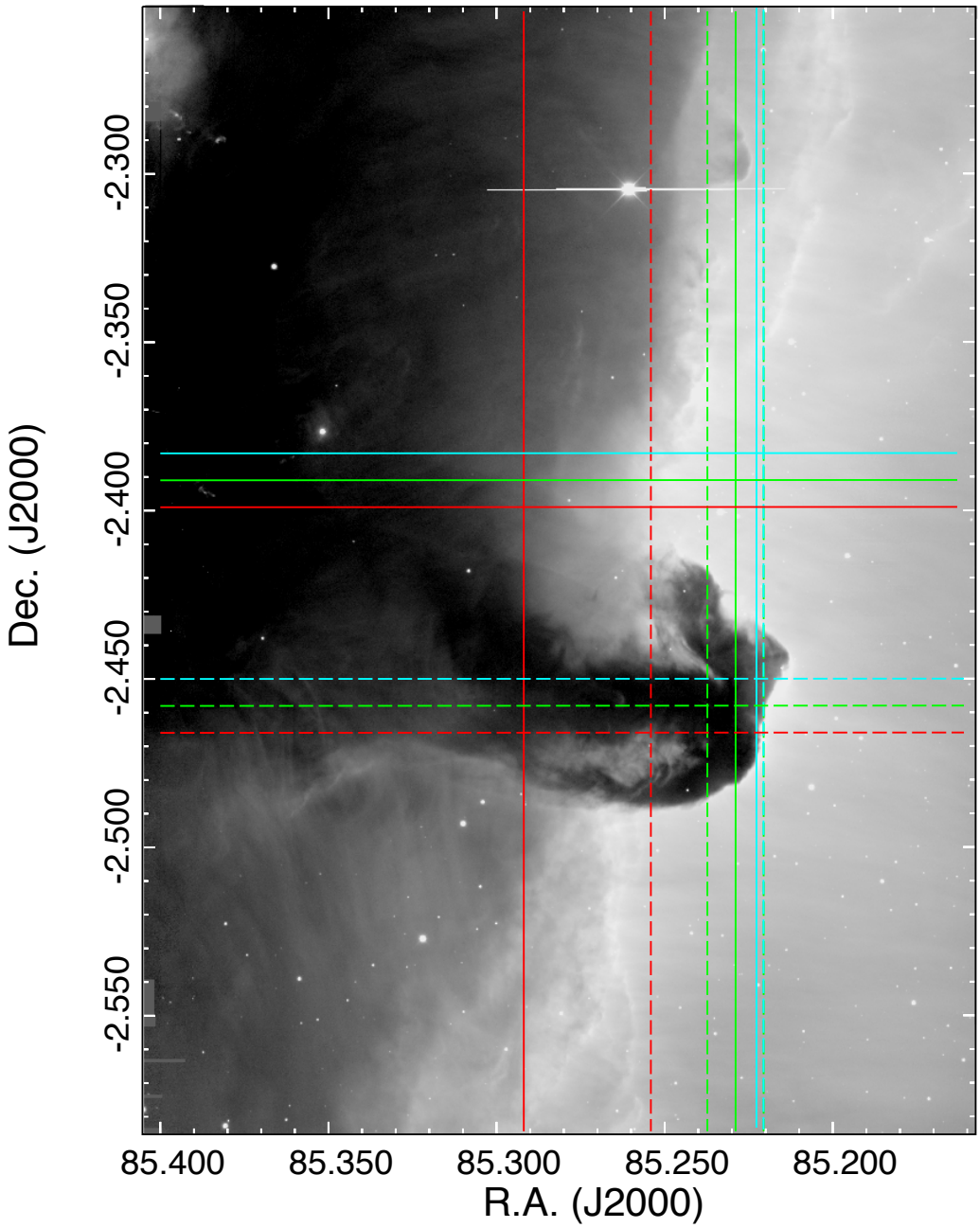

Figure 1. A narrow-band Hα image of the Horsehead Nebula and part of the IC 434 HII region obtained through an 80Å bandpass filter with the Mosaic I CCD on the Mayall 4-meter reflector. The colored lines show the locations of the spatial-velocity diagrams shown in Figures 5 and 6. The long 'neck' of the Horsehead, seen in silhouette, points towards the star σ-Ori located $\sim$35$'$ ($\sim$4 pc) towards the right.

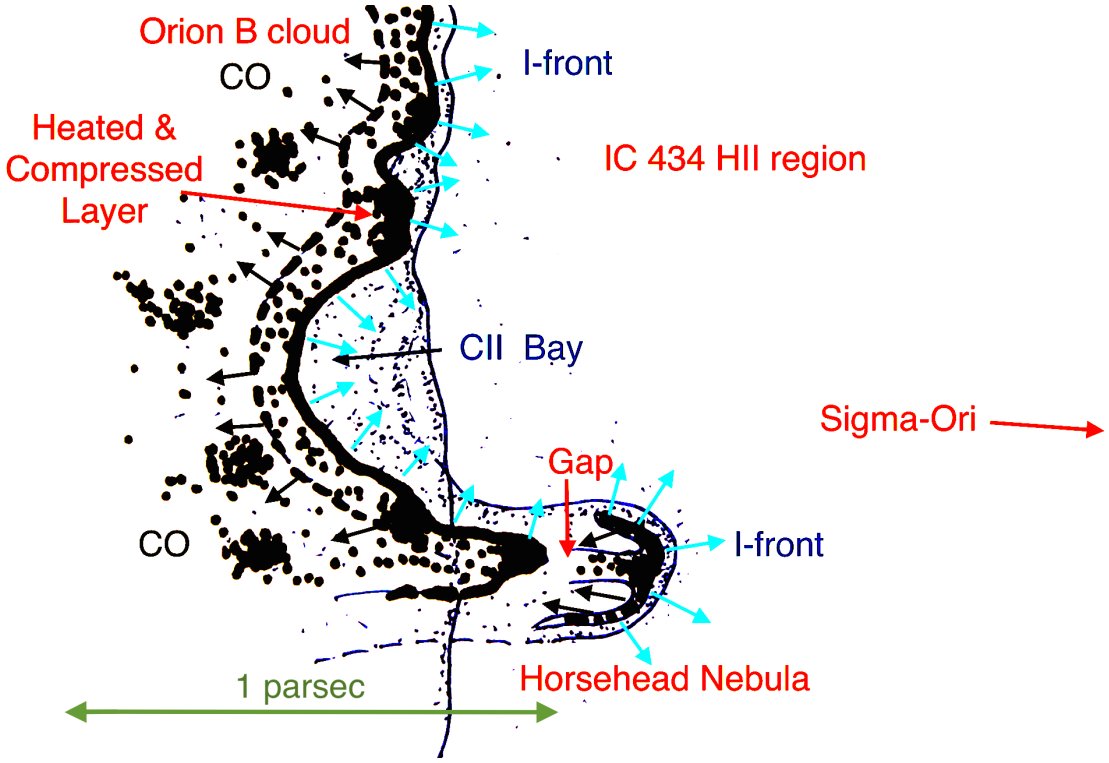

Figure 2. A cartoon showing the likely configuration of the Horsehead Nebula and the IC 434 I-front. Our line-of-sight is from the below and in-front of the figure. σ-Ori is located about 4 pc to the right and slightly behind the plane of the sky from our vantage point. The thin solid line shows the I-front with cyan vectors indicating the approximate direction of the ionized photo-ablation flow. The thick solid line shows the approximate location where CO is dissociated into CI and OI. Most [C^+] emission originated s located between this line and the I-front. The thick dashed line indicates the likely location of the D-type shock or compression wave pushed into the Orion B cloud on the left. The black dotted regions are meant to indicate pre-existing dense clumps in the cloud and the compressed layer between the advancing HII region driven D-type shock or compression wave.

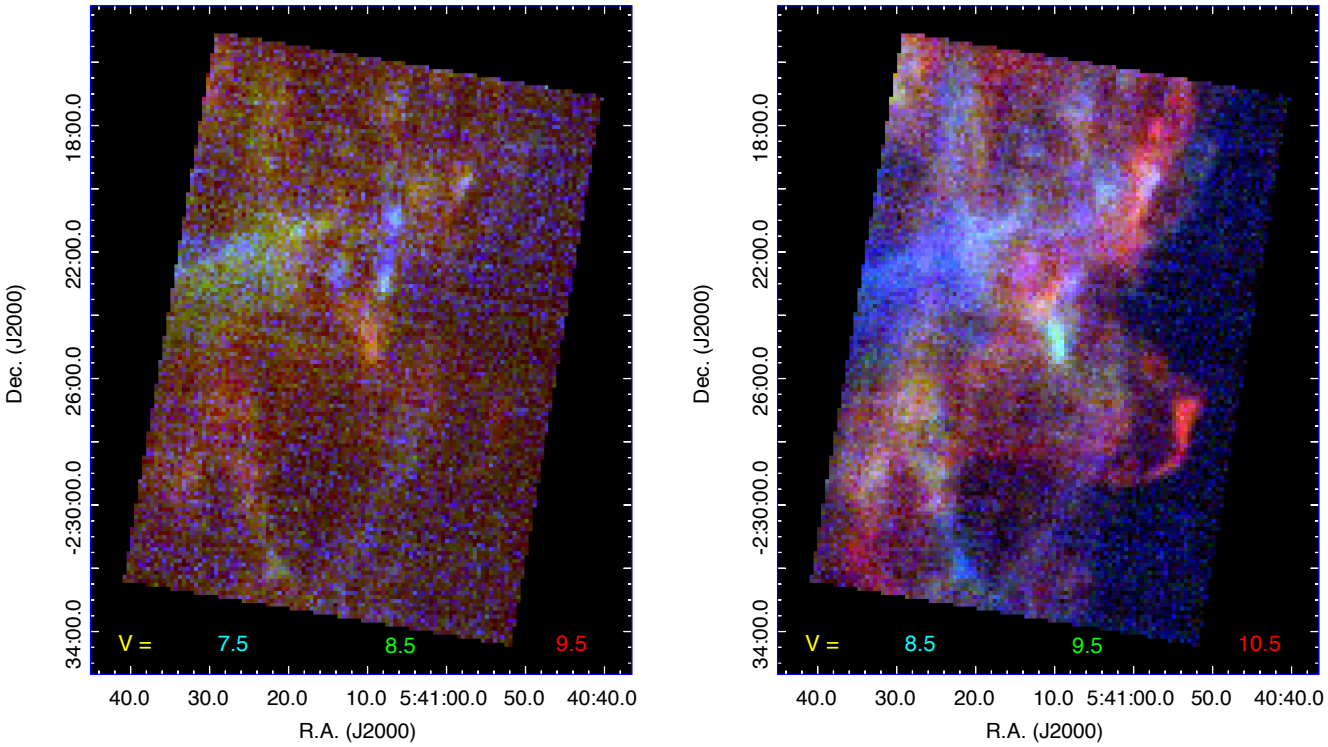

(a)

(b)

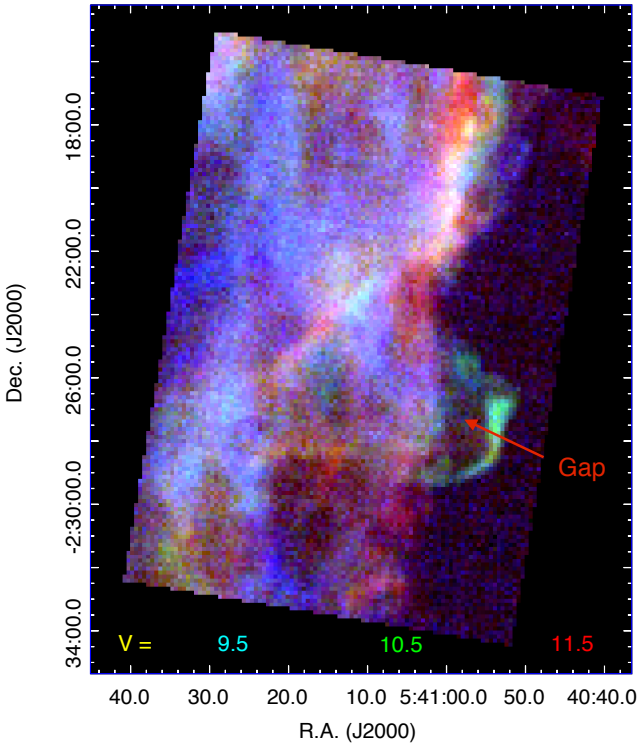

(c)

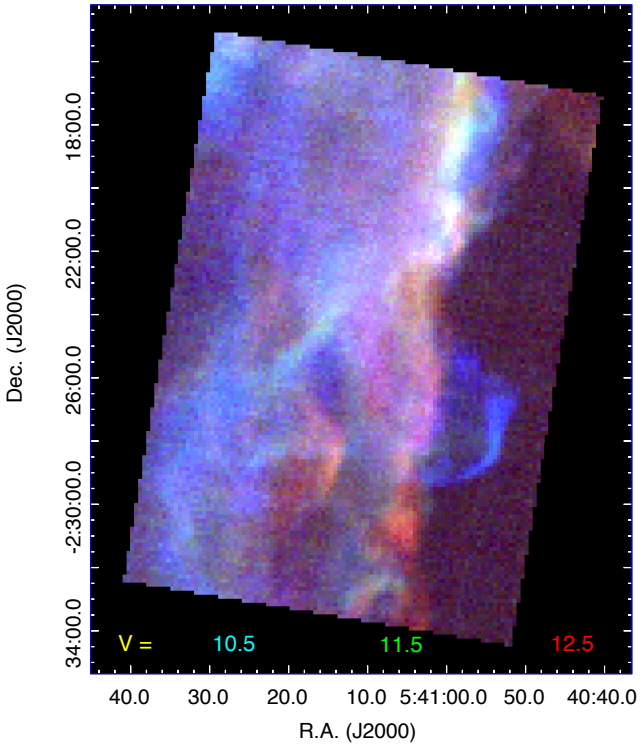

(d)

Figure 3. [C^+] channel maps where each channel has a width of $\Delta V = 1.0$ km s^{-1} shown in three colors. The LSR radial velocities are given in each panel with their respective colors.

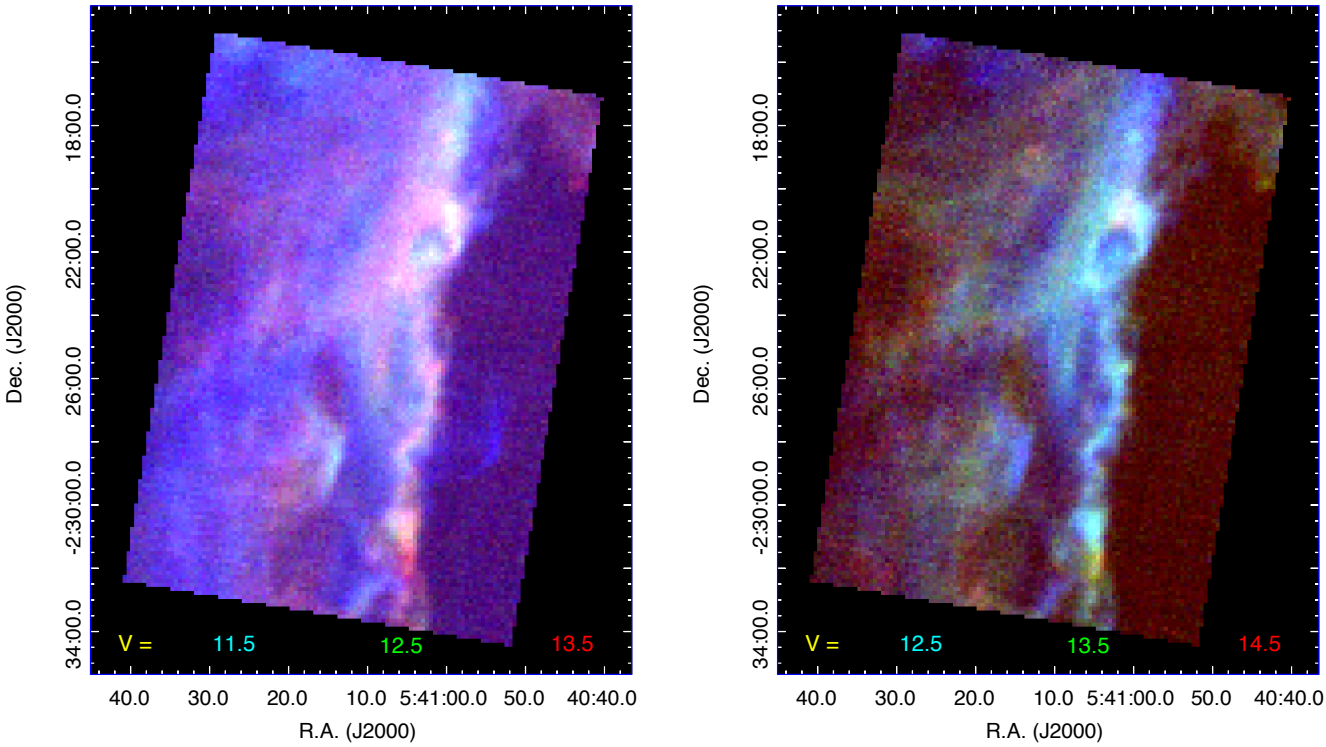

(e)

(f)

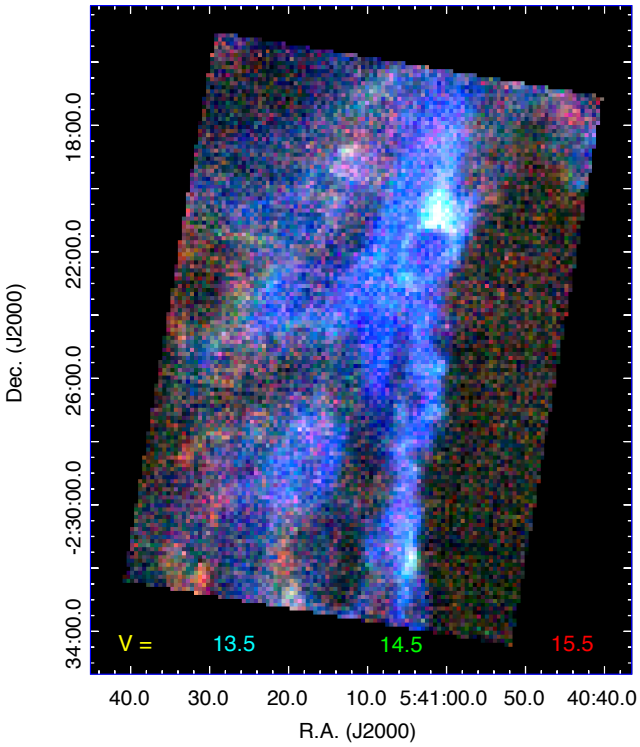

(g)

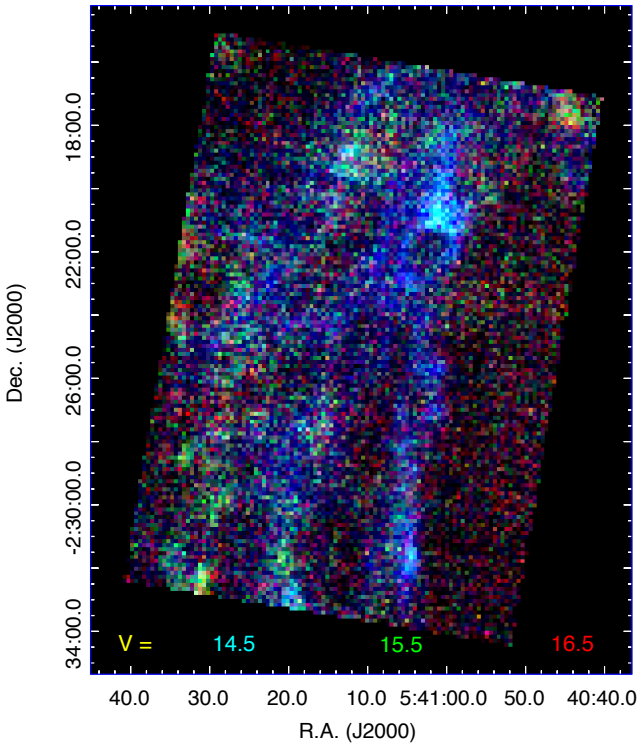

(h)

Figure 4. [C^+] channel maps continued.

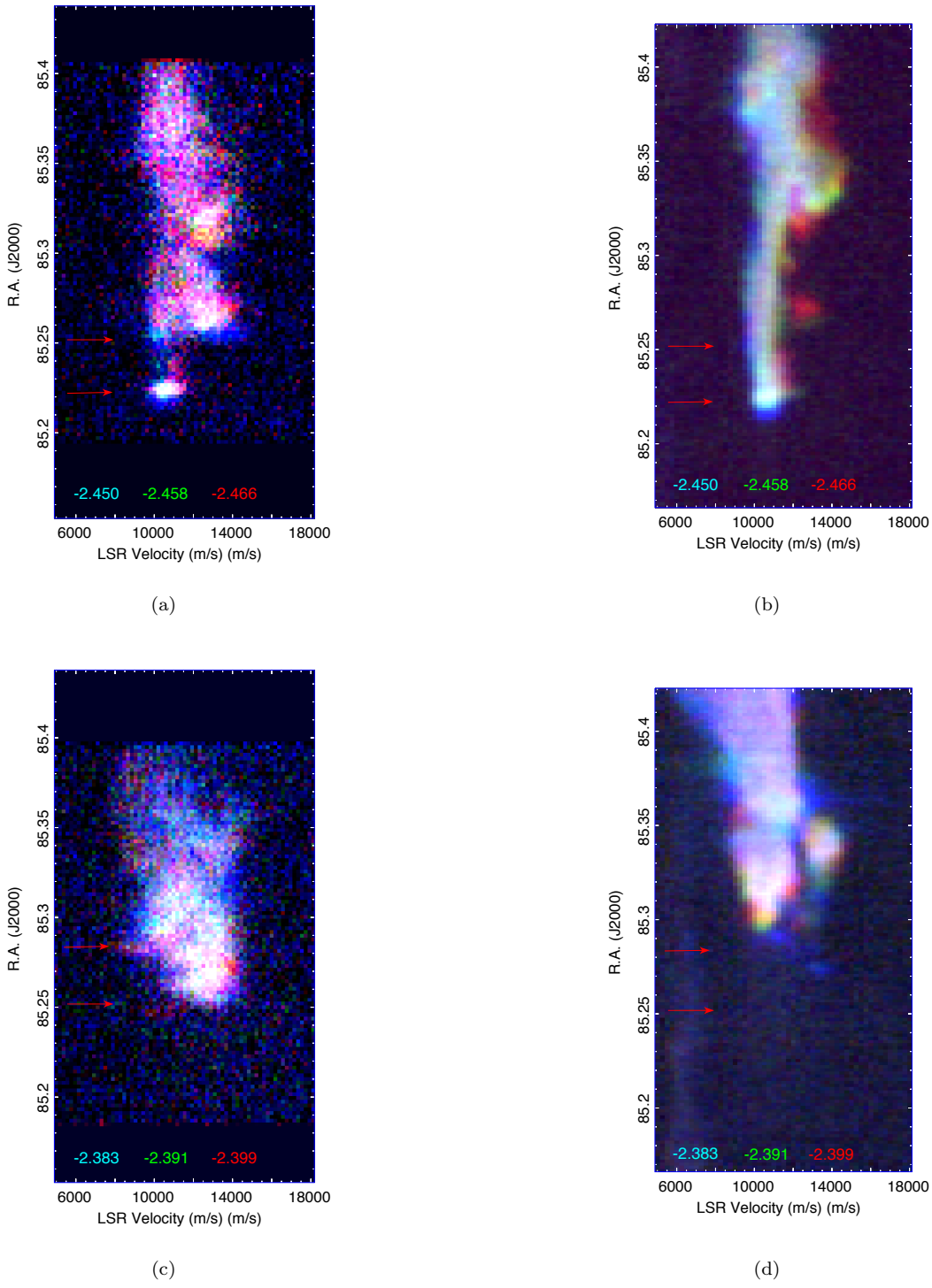

Figure 5. Spatial-velocity (SV) diagrams along the 6 east-west strip indicated by the colored lines in Figure 1. Each panel shows three SV diagrams in blue, green, and red; their Declinations are given by the numbers in their respective colors. The left two panels show [C^+] SV cuts; the right two panels show CO 3−2 emission along the same strips. The top panels show three strips cutting through the Horsehead Nebula (dashed lines in Figure 1; the lower two panels show cuts 4′ to the north (solid lines in Figure 1.

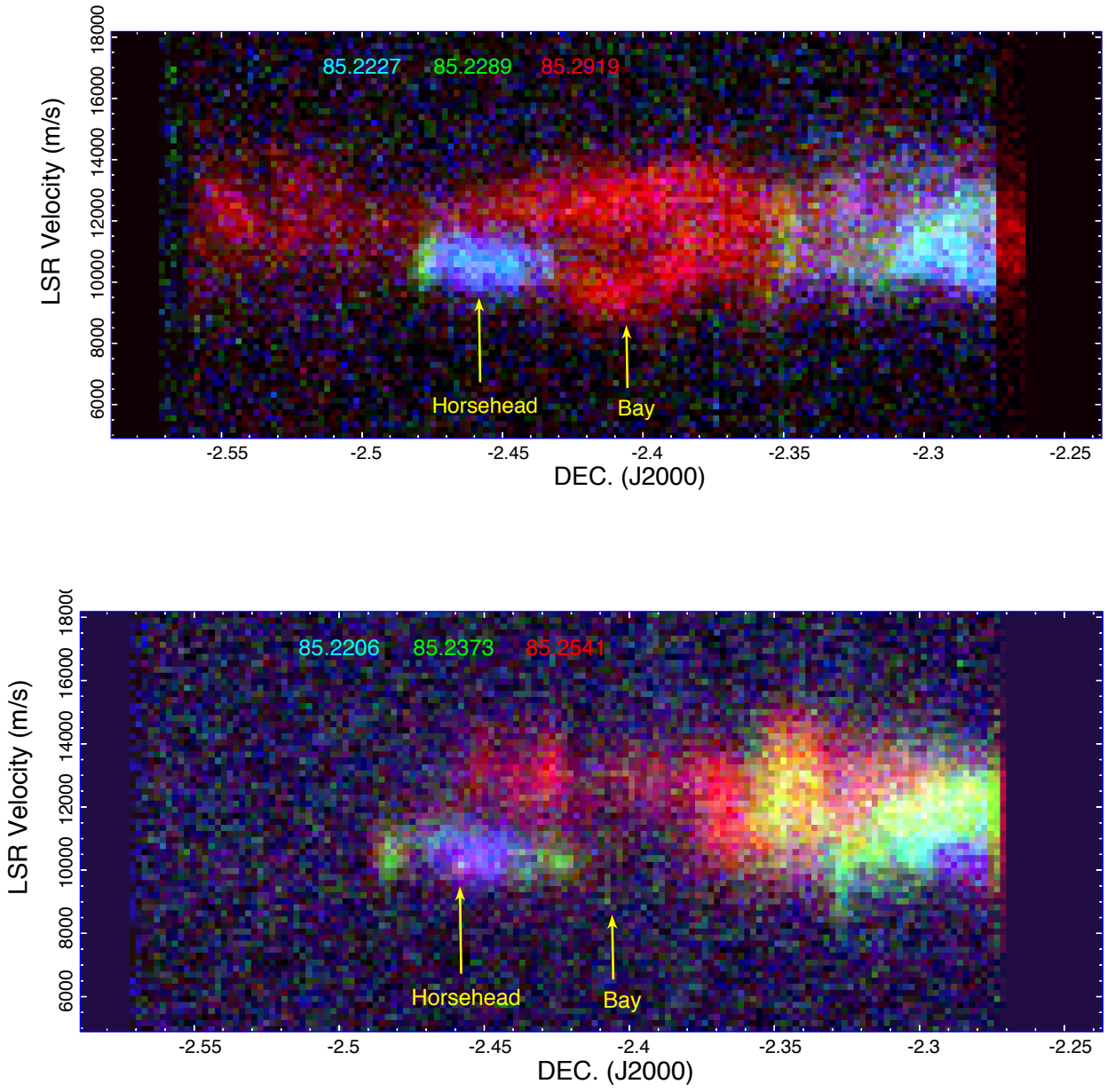

Figure 6. Three-color north-to-south position-velocity diagrams at the Right Ascensions indicated by the blue, green, and red numbers. The locations of the Horsehead and the 'bay' are marked with yellow arrows. The locations of the strips shown at the top are marked with vertical solid lines in Figure 1; vertical dashed lines mark the strips shown at the bottom of this figure. The double-peaked [C^+] emission can be seen in the red (eastern-most) image between the 'bay' and the Horsehead.

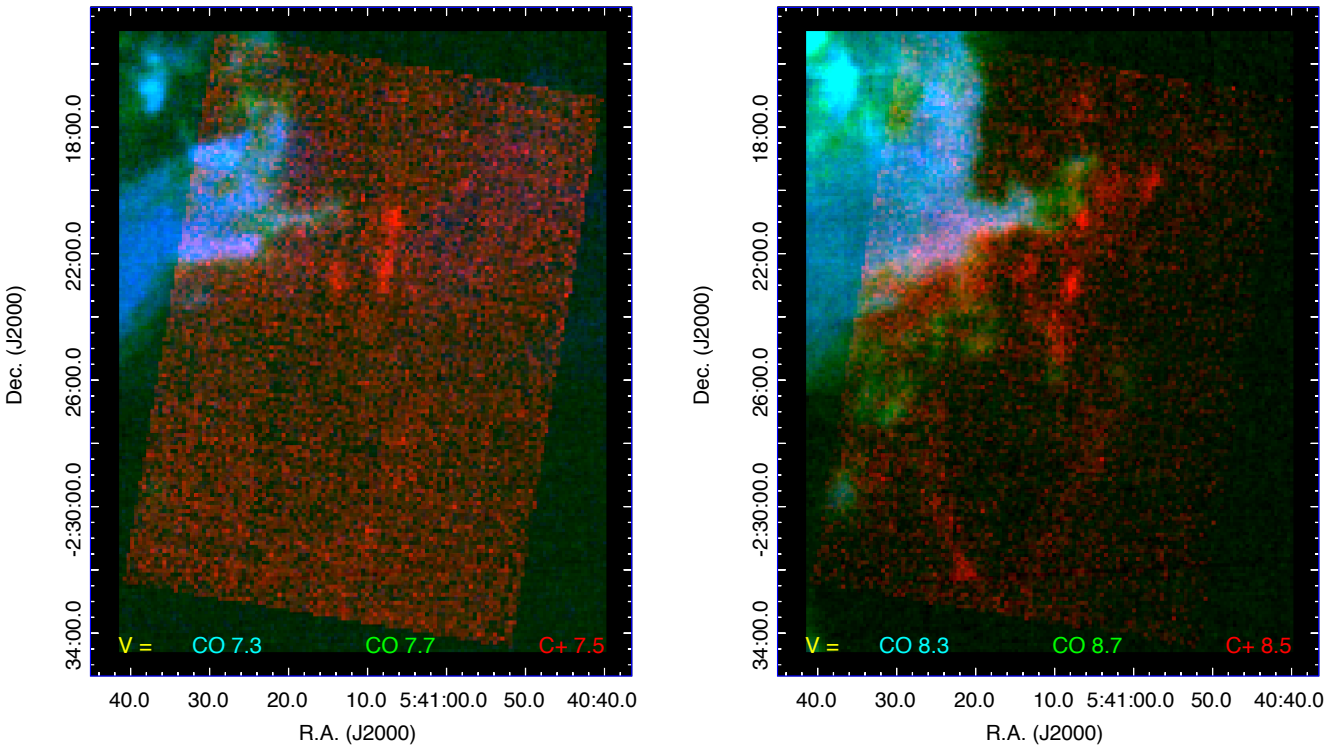

(a)

(b)

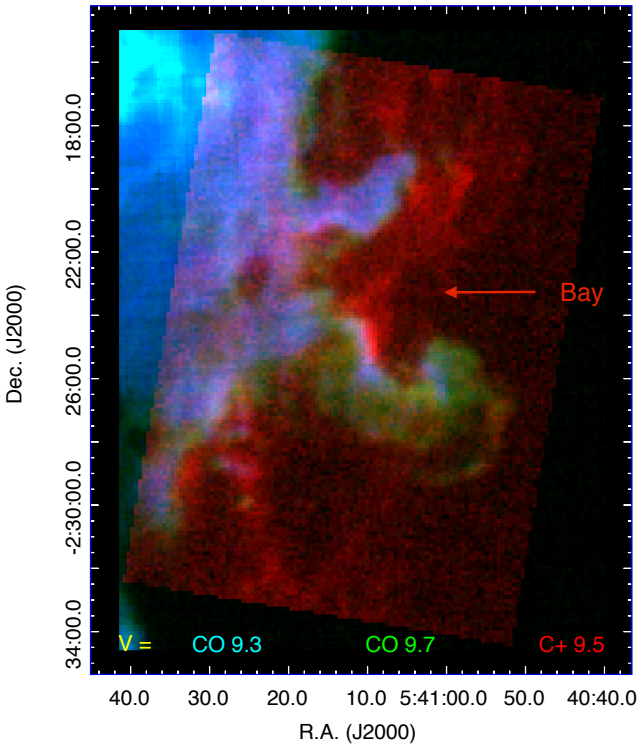

(c)

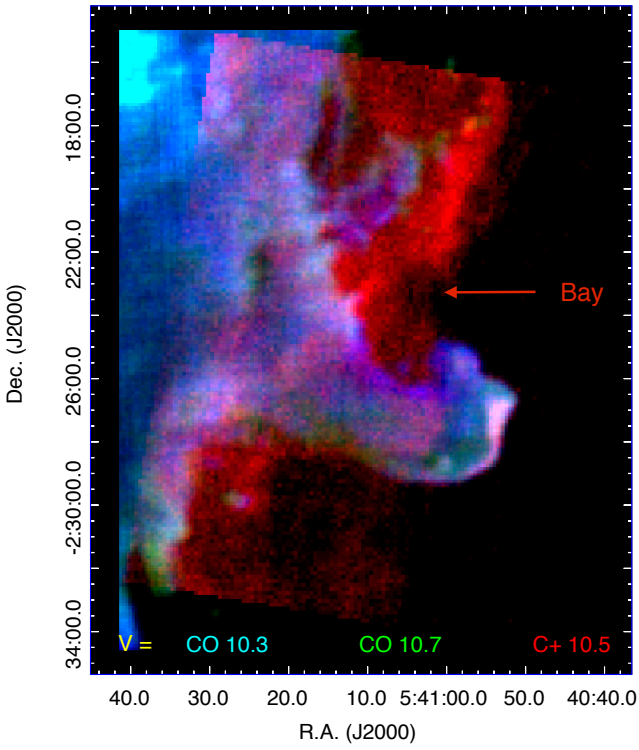

(d)

Figure 7. CO J=3-2 maps in ΔV 0.25 km s^{-1}-wide channels centered on the LSR radial velocities indicated by the cyan and green numbers, shown in those colors respectively, superimposed on the [C$^+$] emission in ΔV = 1.0 km s^{-1}-wide wide channels shown in red, centered on the LSR radial velocity indicated in the red numbers.

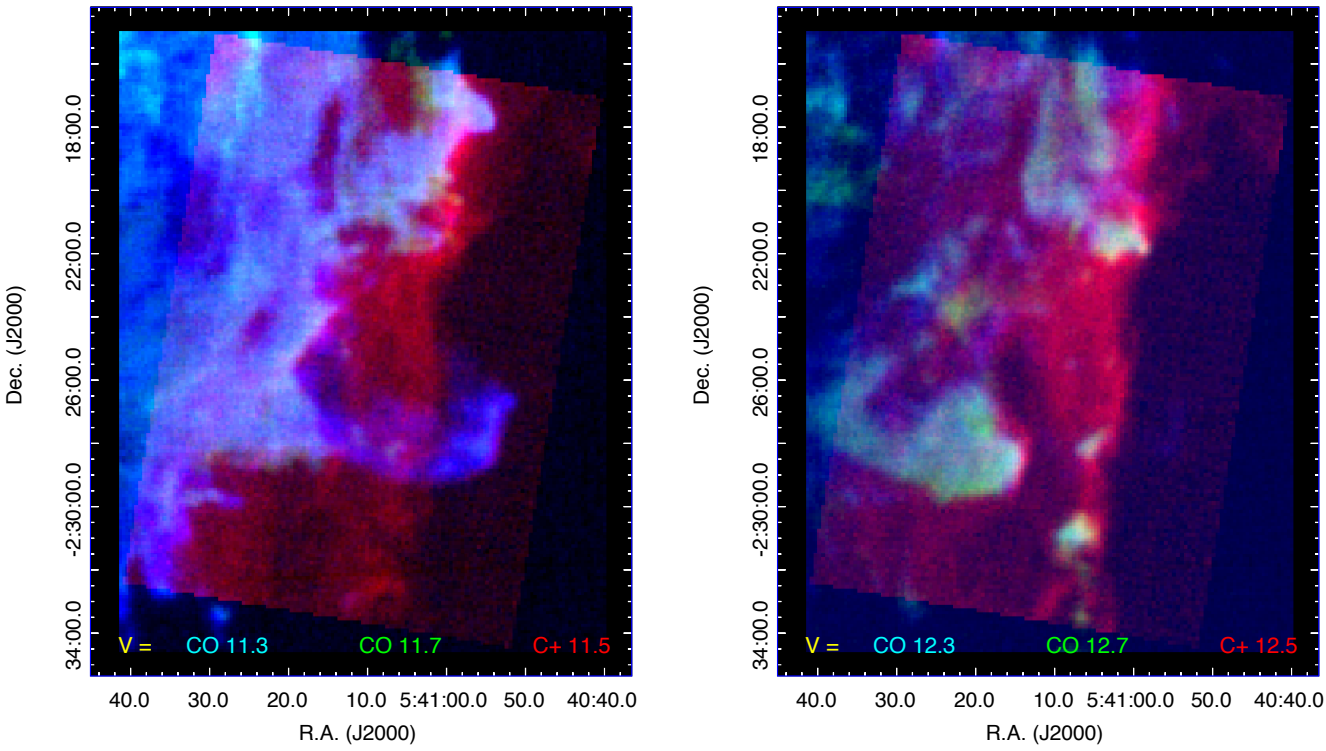

(e) (f)

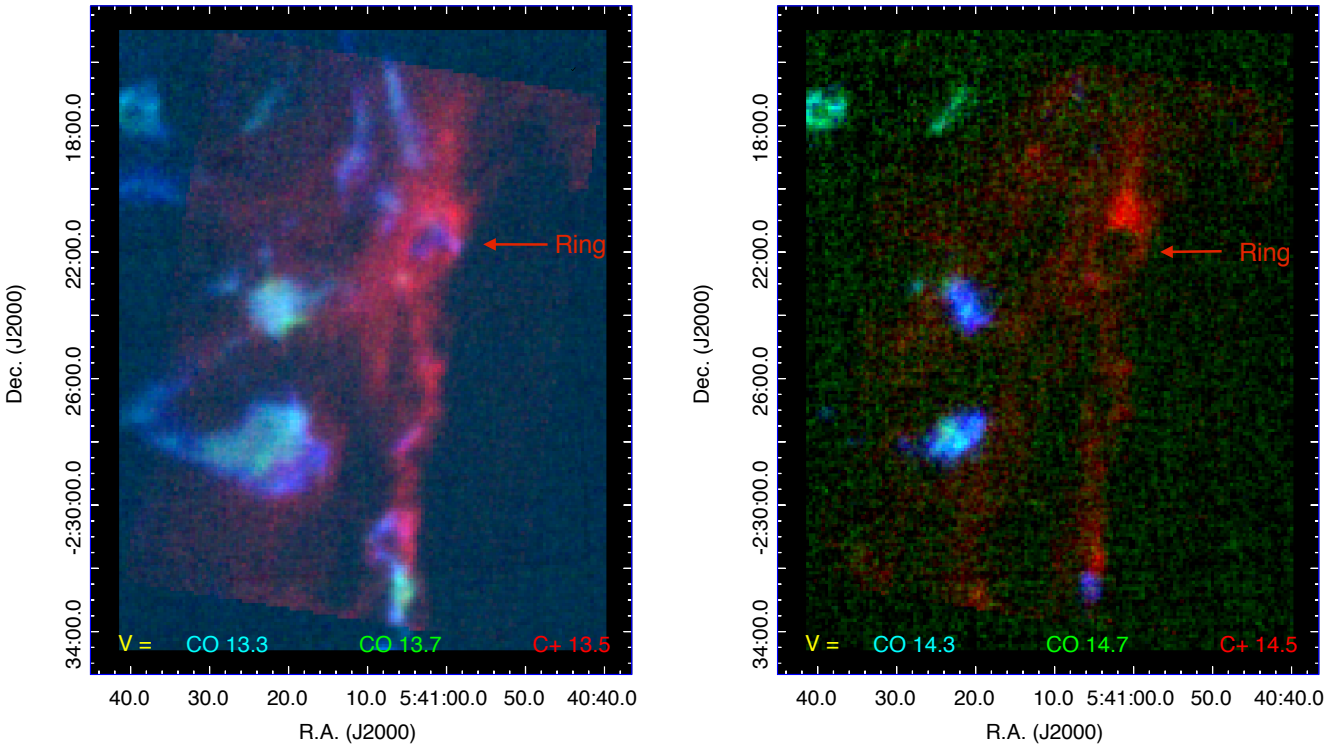

(g) (h)

Figure 8. Figure 7 continued.

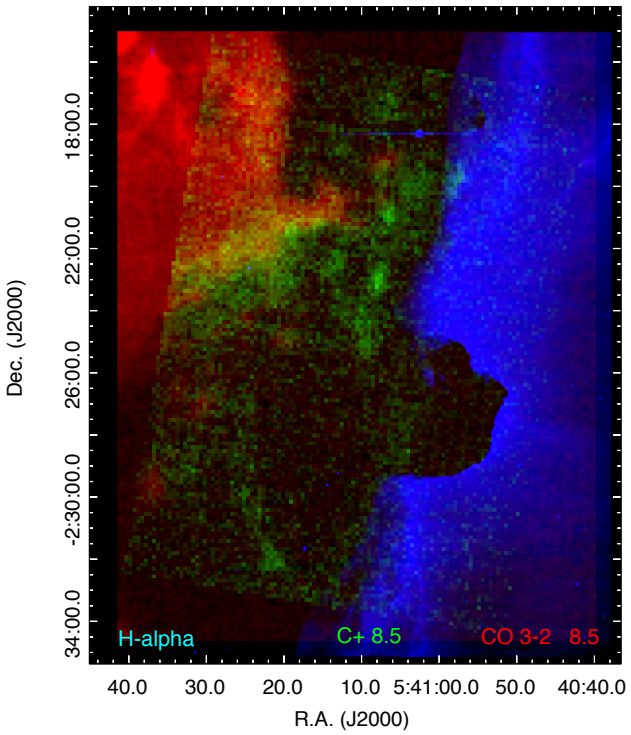

(a)

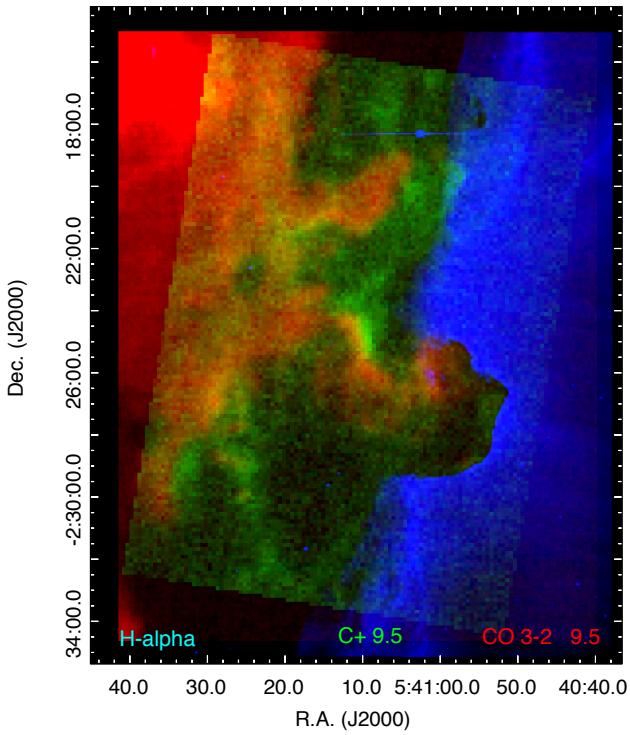

(b)

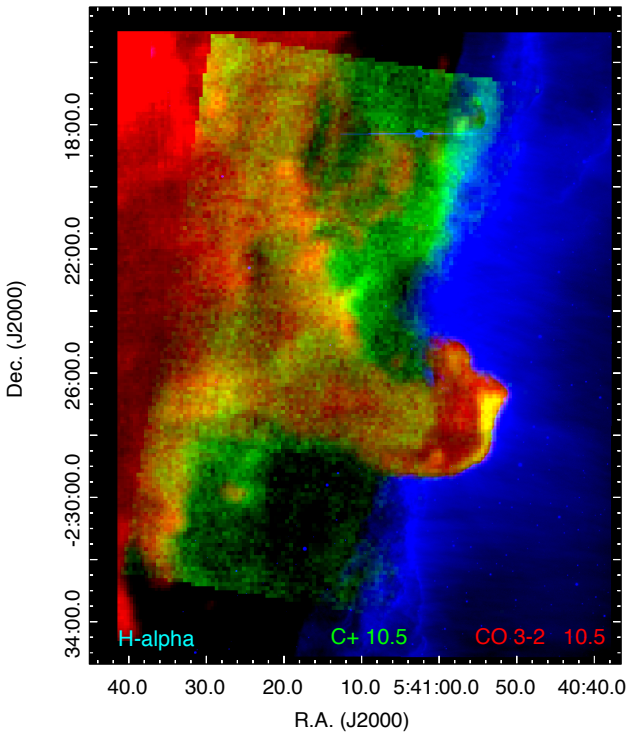

(c)

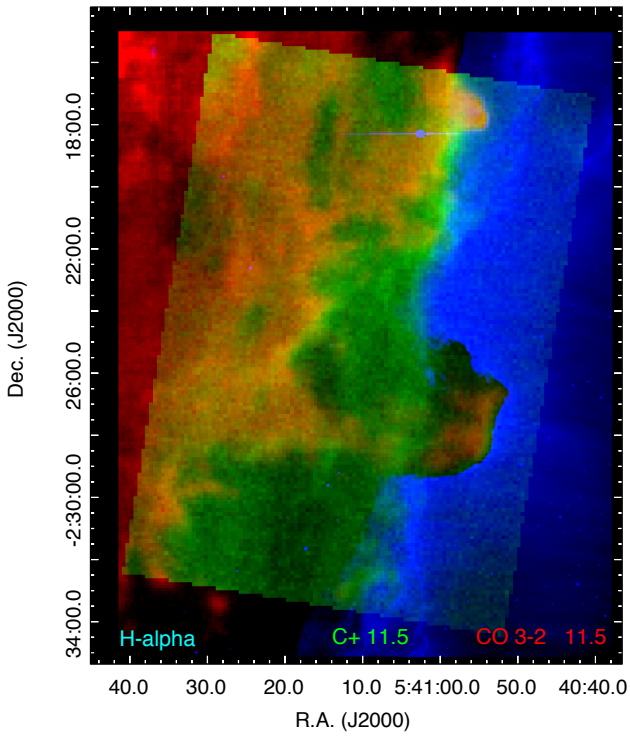

(d)

Figure 9. The Horsehead Nebula in Hα (blue), C^+ (green) in $\Delta V = 0.96$ km s^{-1} channels , and CO 3-2 (red) in $\Delta V = 0.25$ km s^{-1} channels. The LSR velocities in km s^{-1} are indicated in the corresponding green an red numbers.

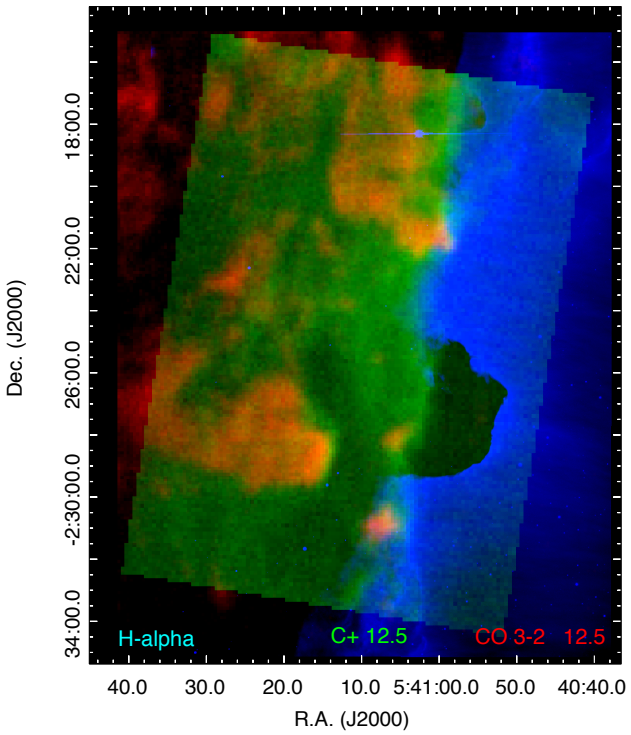

(e)

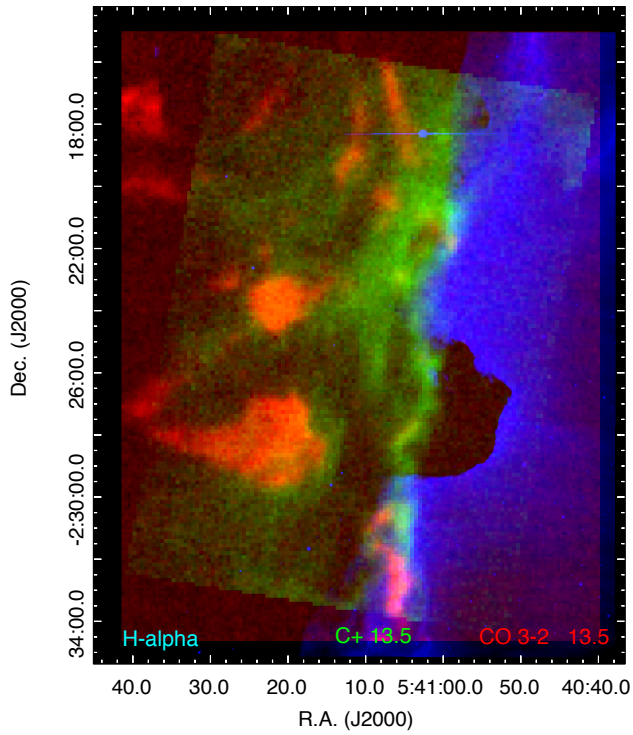

(f)

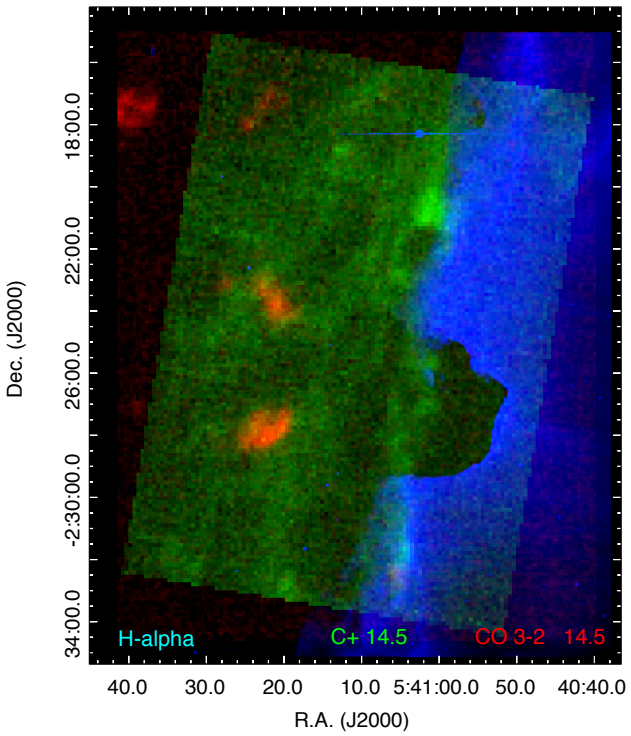

(g)

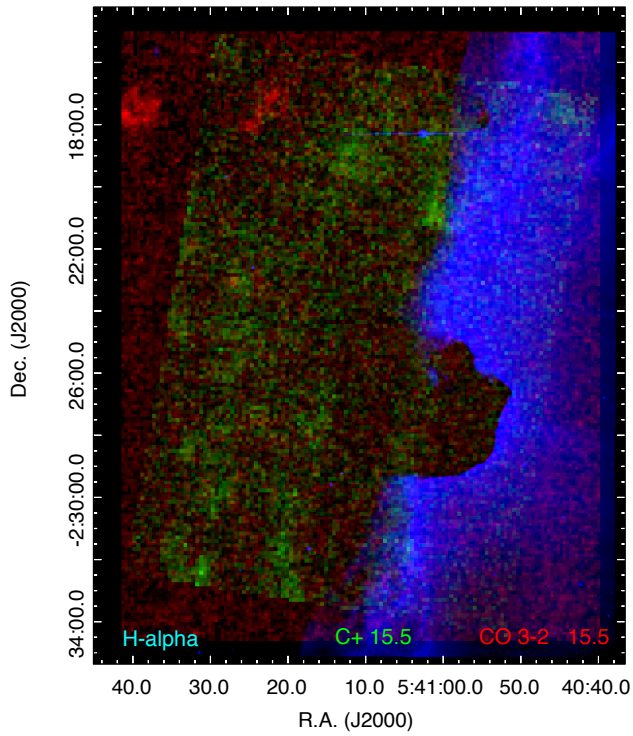

(h)

Figure 10. Figure 9 continued.

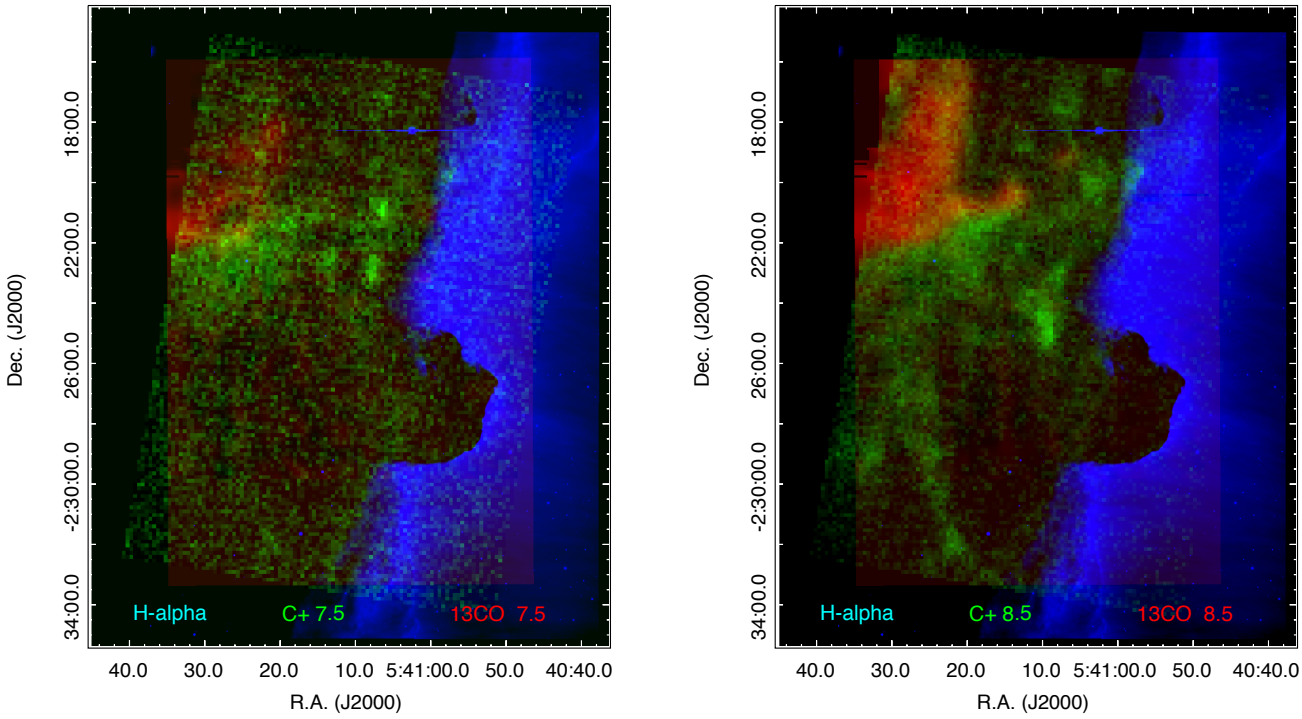

(a)

(b)

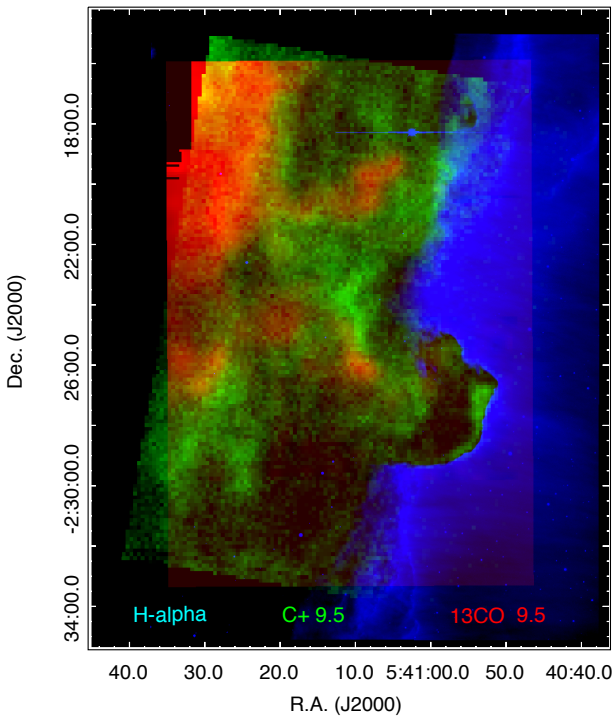

(c)

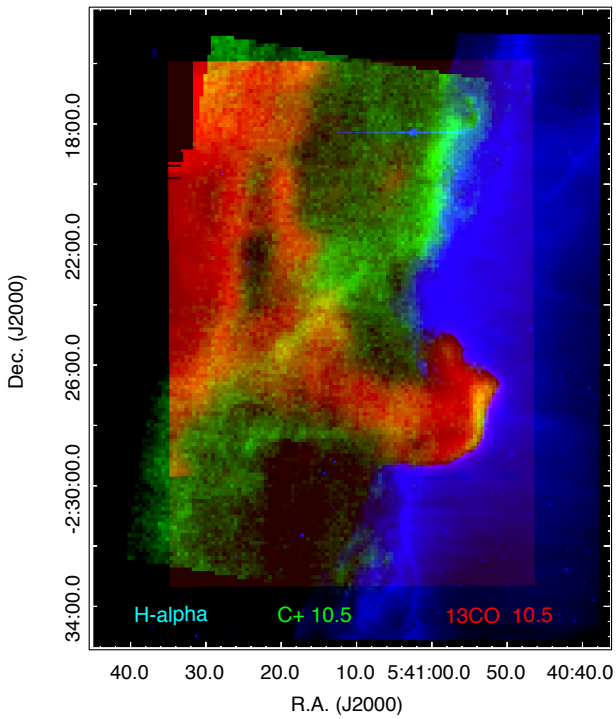

(d)

Figure 11. The Horsehead Nebula in Hα (blue), C^+ (green) in $\Delta V = 0.96$ km s^{-1} channels , and ^{13}CO 2-1 (red) in $\Delta V = 0.1$ km s^{-1} channels. The LSR velocities in km s^{-1} are indicated in the corresponding green an red numbers.

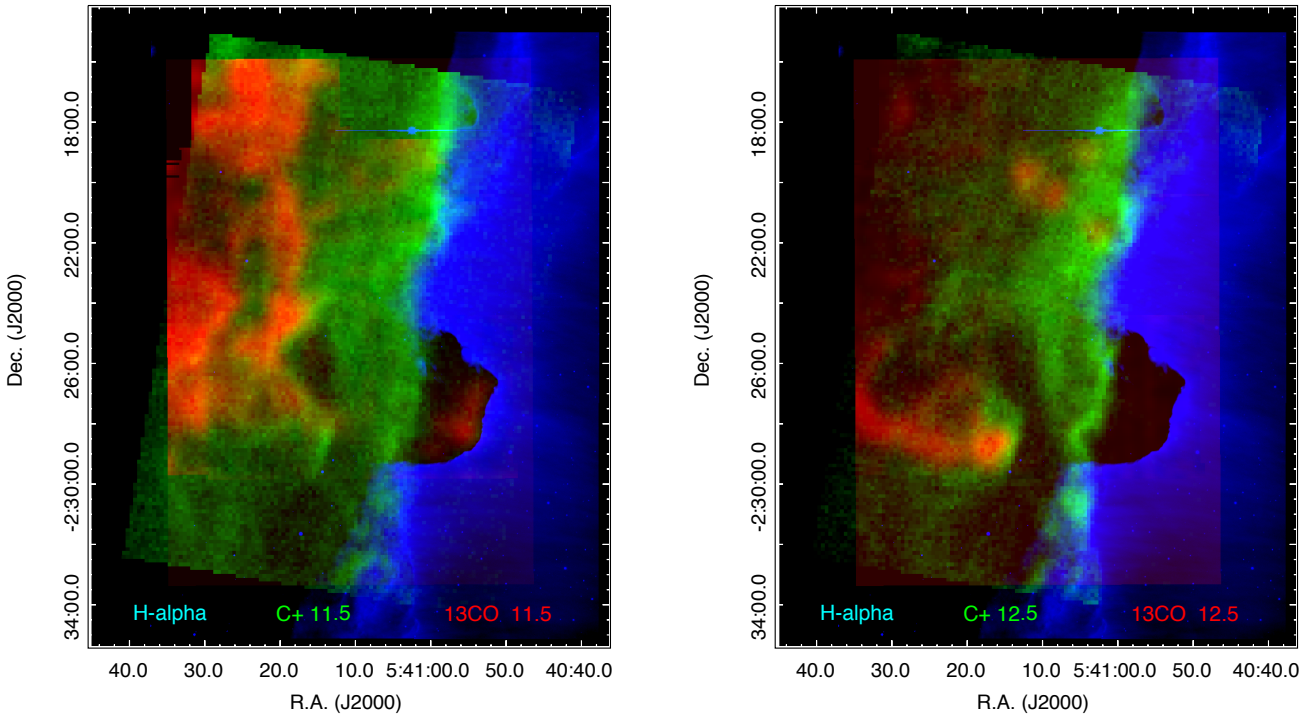

(e)

(f)

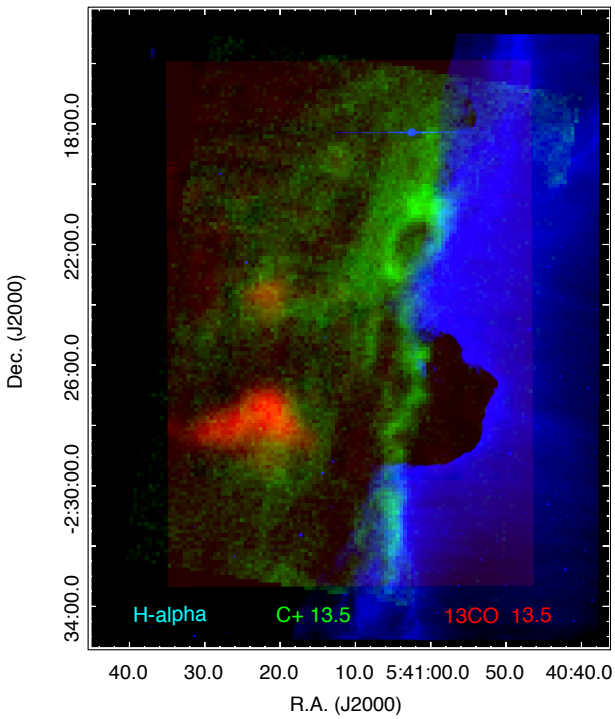

(g)

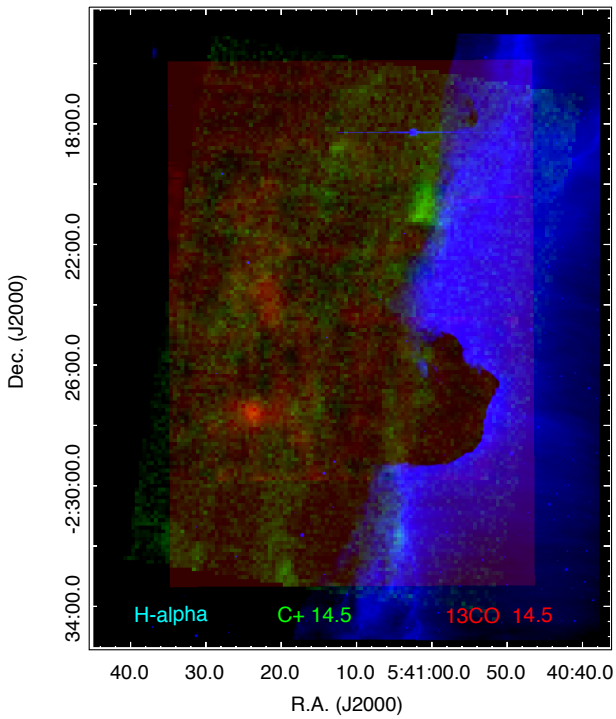

(h)

Figure 12. Figure 11 continued.

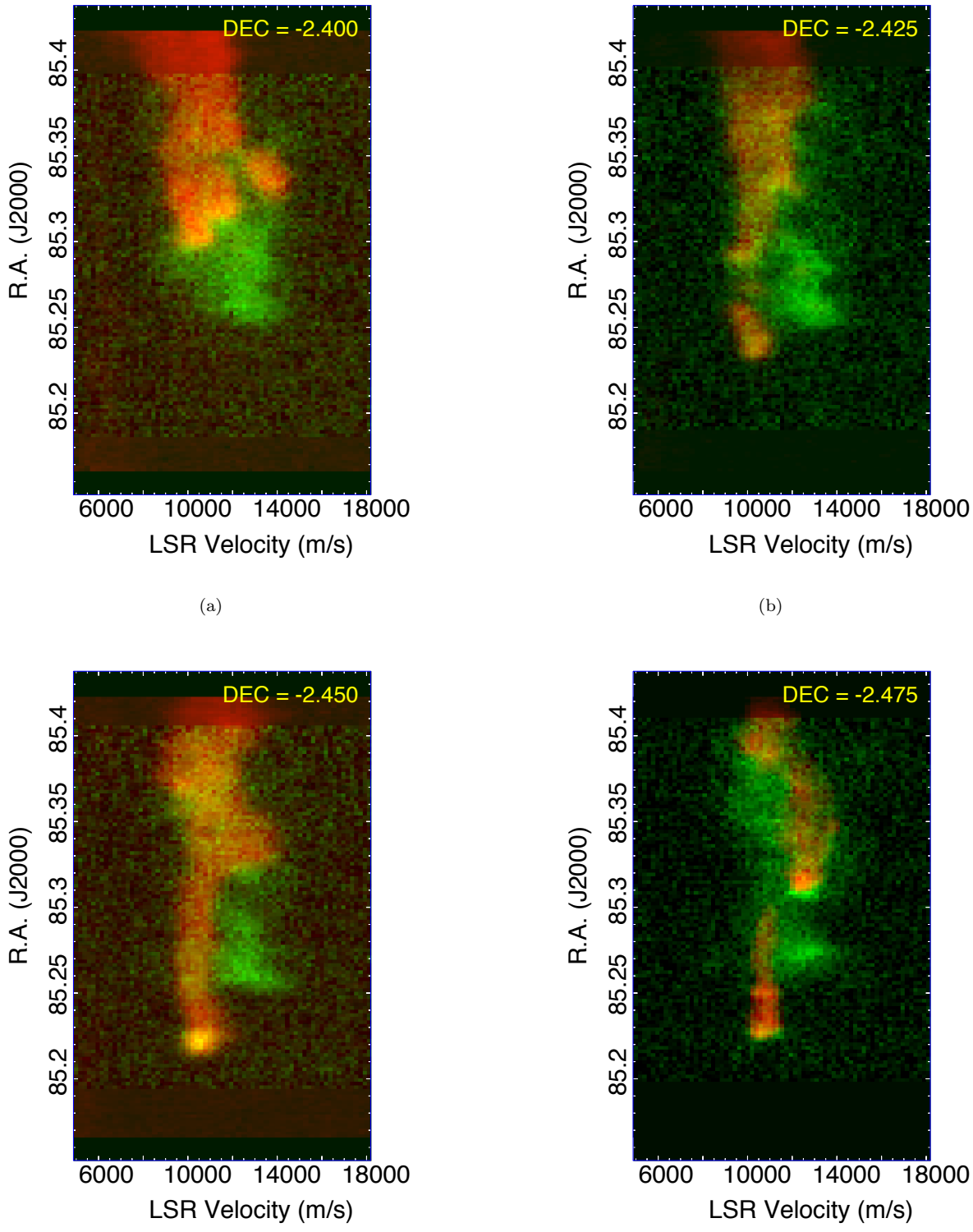

Figure 13. Radial velocity vs. R.A. cuts at various Declinations indicated in the panels showing ^{12}CO 3-2 in red and [C^{+}] 157 μm in green. These 4 panels show cuts through the Horsehead Nebula.

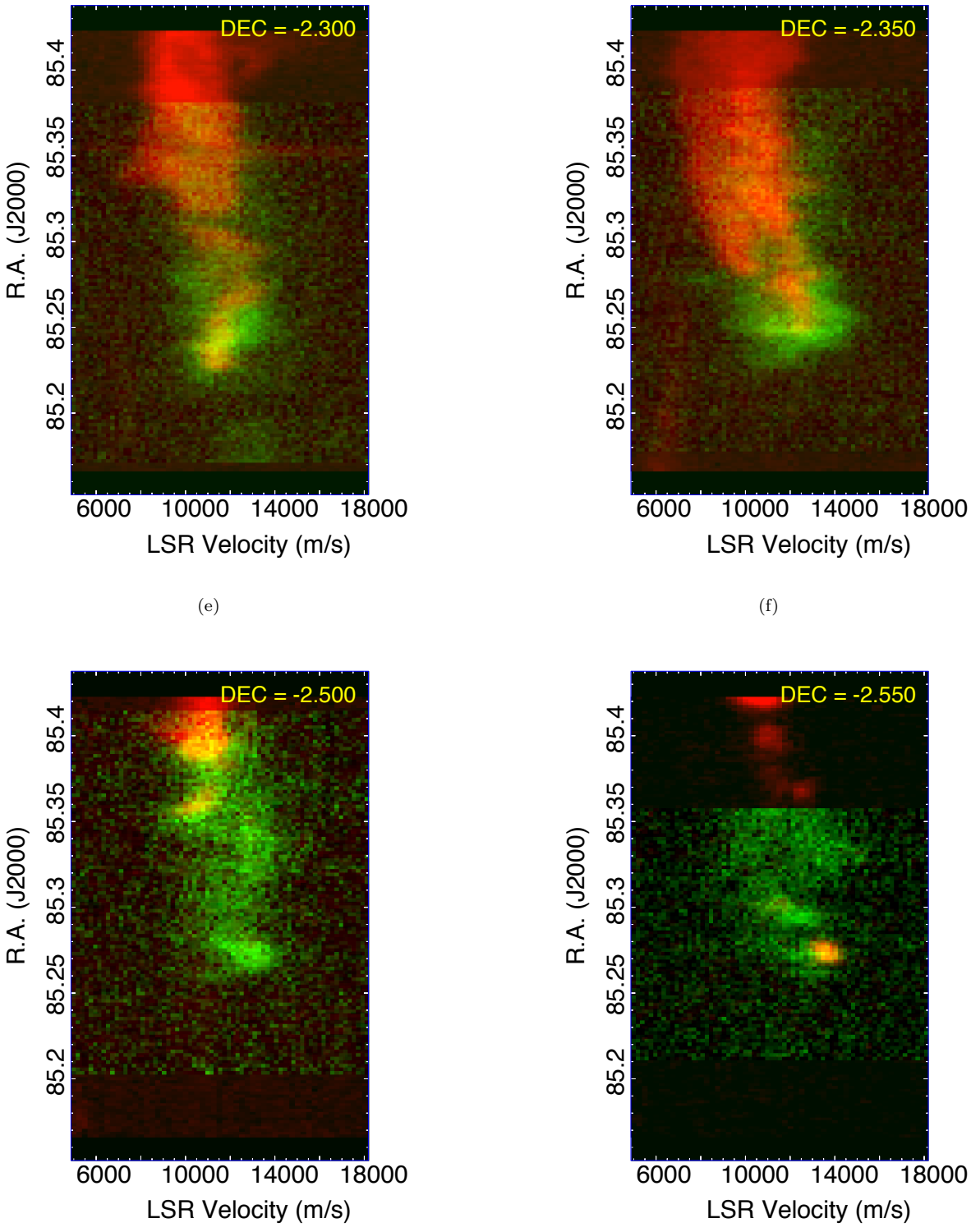

(e) (f)

(g) (h)

Figure 14. Radial velocity vs. R.A. cuts at various Declinations indicated in the panels showing ^{12}CO 3-2 in red and [C$^+$] in green. These 4 panels show cuts through the IC 434 I-front north of the Horsehead Nebula (top two panels) and south of the Horsehead Nebula (bottom two panels).

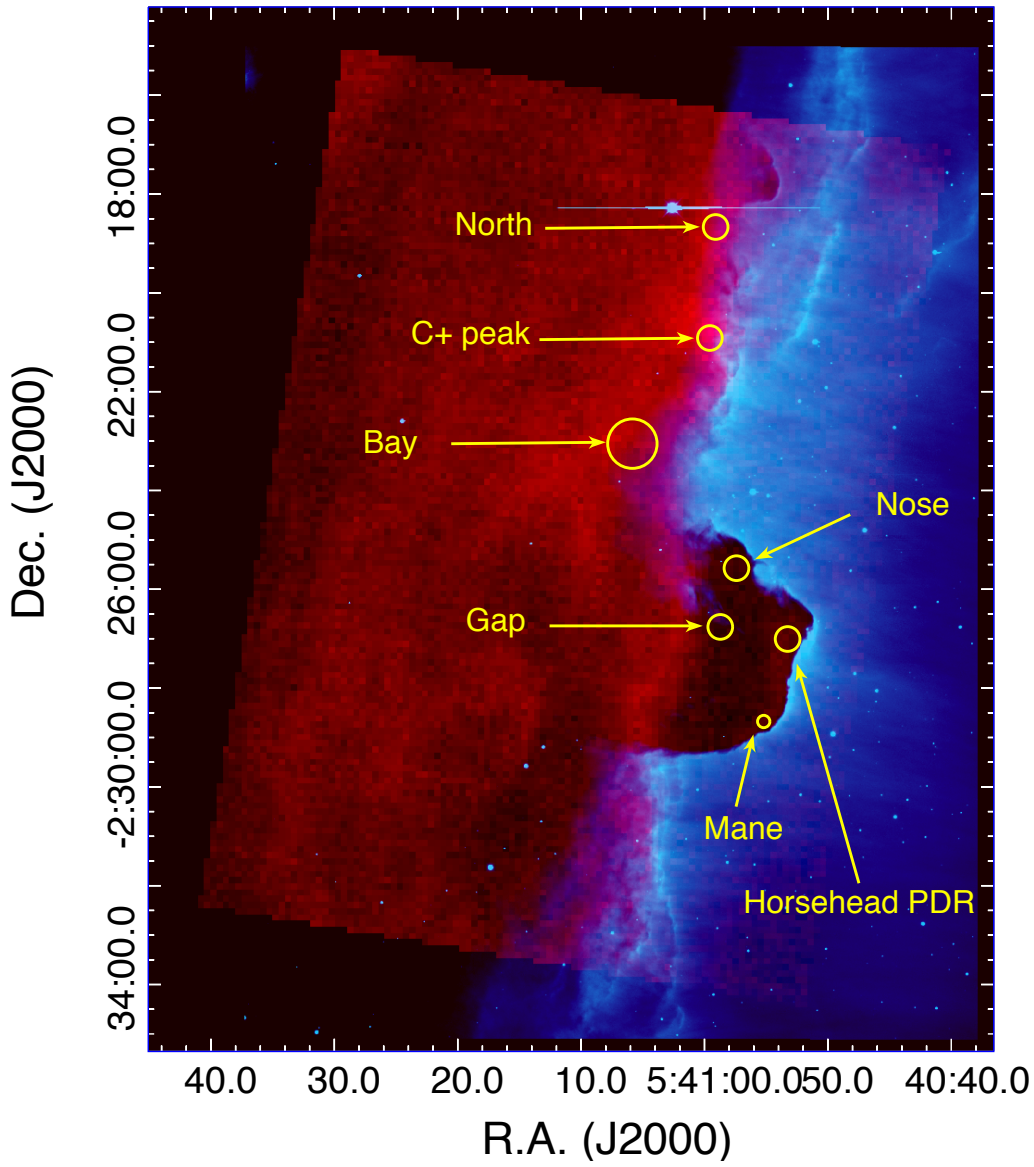

Figure 15. Image showing the [C$^+$] emission integrated from V_{LSR} = 7 to 27 km s^{-1}(red) superimposed on the Hα image. The yellow circles mark the locations and sizes of the regions over which the [C$^+$] line emission was measured and converted into column densities listed in Table 1.